

Vector boson scattering at the LHC

A study of the $WW \rightarrow WW$ channels with the Warsaw cut

M. Fabbrichesi[†], M. Pinamonti^{‡*}, A. Tonerio[°], and A. Urbano^{†*}

[†]*INFN, Sezione di Trieste*

[‡]*INFN, Sezione di Trieste, Gruppo collegato di Udine*

^{*}*SISSA, via Bonomea 265, 34136 Trieste, Italy and*

[°]*ICTP-SAIFR, Rua Dr. Bento Teobaldo Ferraz 271, 01140-070 São Paulo, Brazil*

(Dated: November 15, 2021)

We study W boson scattering in the same- and opposite-sign channels under the assumption that no resonances are present in the collider processes $pp \rightarrow l^\pm \nu_l l^\pm \nu_l jj$ and $pp \rightarrow l^\pm \nu_l l^\mp \nu_l jj$, respectively. Basic selection cuts together with a restriction on the combination of the final lepton and jet momenta (the Warsaw cut) makes it possible to argue that at the LHC a luminosity of 100 fb^{-1} and a center-of-mass energy of $\sqrt{s} = 13 \text{ TeV}$ will allow to constrain the leading effective lagrangian coefficients at the permil level. We also discuss limits on the other coefficients of the effective lagrangian as well as stronger constraints provided by higher energy and luminosity. We show that the same-sign $WW \rightarrow WW$ channel suffices in providing the most stringent constraints.

PACS numbers: 12.60.Cn

I. INTRODUCTION

Vector boson scattering (VBS) at the LHC provides a direct window on the mechanism responsible for the breaking of the electroweak (EW) symmetry. The tree-level amplitude for VBS is the combination of seven subprocesses in which gauge and Higgs bosons are exchanged. In the standard model (SM) the terms leading in energy cancel leaving an amplitude and a cross section consistent with unitarity. If any or all among the trilinear and quartic gauge couplings and the Higgs boson coupling to the vector bosons are modified these delicate cancellations fail and tree-level unitarity is lost. In particular, if either the trilinear or the quartic gauge couplings are changed, terms proportional to the fourth power of the center-of-mass (CM) energy will be present.

After the existence of the Higgs boson has been confirmed [1], we know that this particle plays a role in EW symmetry breaking but the details may differ from the basic scenario in which the Higgs boson is linearly and minimally coupled. If the gauge couplings are left unchanged but the Higgs boson couplings to the vector bosons are modified, terms proportional to the square of the CM energy will be present in the amplitude for VBS.

All these potential departures from the SM represent signals for new physics. Since there are many possibilities—ranging from an extended Higgs sector to strong dynamics—they are best described by means of an effective field theory.

Terms in the amplitude growing with the CM energy arise when considering the scattering among the longitudinal components of the vector bosons. Using the equivalence theorem [2], these components can be identified with the Goldstone bosons of the EW symmetry breaking and behave as scalar particles with derivative couplings: their scattering amplitudes are similar to those for $\pi\pi$ -scattering in QCD and the same techniques can be used. The transverse components give rise to terms in the amplitude that are bounded in the CM energy and subleading—for all practical purposes, they are part of the background. The natural language for computing the relevant amplitudes is that of the effective nonlinear (chiral) EW lagrangian first introduced in [3].

Depending on the symmetry group used, there exist different effective lagrangians which are equivalent but differ in the order-by-order terms and therefore in the dimension and field content of the operators. Compared to other effective lagrangian based on the linear theory and the full symmetry group, the chiral EW lagrangian has the advantage of being optimised for VBS.

The loss of tree-level unitarity suggests the presence of a strongly interacting sector. We expect unitarity to be restored by the presence of resonances. Barring the spectacular case of the LHC actually seeing one or more of these resonances, this loss and its eventual restoration can be studied by the effective EW lagrangian in terms of bounds of its coefficients. Because we now know that the theory also contains a Higgs boson, such a lagrangian must be completed by the introduction of this field [4, 5]—the effect of which is parameterised in terms of additional coefficients.

The same-sign $W^\pm W^\pm \rightarrow W^\pm W^\pm$ channel stands out in this search because of the suppressed QCD background and the reduced contribution from channels where transverse and longitudinal gauge bosons are mixed. It is a channel in which is easier to single out the scattering of the longitudinal components of the gauge bosons and the most likely

place to look for possible deviations from the SM.

Possible resonances in this channel are expected to be either present in the t -channel (and therefore leading to only a decrease of the cross section) or carrying isospin 2 and doubly charged and therefore heavier than those in other decay channels. Under the assumption that no resonance has been seen in this or other channels, it is reasonable to unitarize the amplitude by the simplest and model-independent means without worrying about the value of the resonances' masses and widths. Experimental cross sections for the process $pp \rightarrow l^\pm \nu_l l^\pm \nu_l jj$ can then be compared with the SM and provide the means to constrain the coefficients of the effective lagrangian and the physics behind the EW symmetry breaking.

Even in the same-sign WW channel, the extraction of the coefficients is challenging. Appropriated selection cuts are required to isolate the VBS process from other, often larger backgrounds. In addition, we want to isolate the longitudinally from the transversally polarised vector boson. The former is mostly produced together with a final quark which is more forward than in the case in which the W is transversally polarised. These requirements provide a standard set of selection rules to which we add a final requirement (the Warsaw cut [6]) on the size and direction of the final transverse momenta of jets and leptons which has been shown to be effective in disentangling longitudinal and transverse vector boson polarizations.

The opposite-sign $W^\pm W^\mp \rightarrow W^\pm W^\mp$ channel is less clean mainly because of the large background generated by the production of $t\bar{t}$ pairs. It would be best to do without it and we find that indeed it is possible to establish the most stringent constraints by means of only the same-sign channel.

The study of the cross sections $\sigma(pp \rightarrow l^\pm \nu_l l^\pm \nu_l jj)$ and $\sigma(pp \rightarrow l^\pm \nu_l l^\mp \nu_l jj)$ at the LHC can lead to either the discovery or the exclusion of the terms in the effective lagrangian at the permil level. This is the size of these coefficients expected on dimensional grounds. For the first time we will be able to study the breaking of the EW symmetry at its fundamental level.

In this introduction we recall the relevant literature in section IA, introduce the notation in section IB, discuss coefficients size and higher-order terms in section IC, compare the nonlinear (chiral) lagrangian with the linear and anomalous couplings formulations to provide a dictionary for the relevant coefficients in section ID. We collect the existing limits and estimates in section IE.

A. The story so far

The importance of VBS in the study of the EW symmetry breaking was recognised early on [2, 7]. The unique role played by the same-sign channel was singled out in [8] and the identification of the central jet veto to distinguish the EW signal from the QCD background was first introduced in [9] where the purely leptonic “gold-plated” decay channels were also identified. In [10] the study was extended to semi-leptonic decay modes.

More recently, with the coming of the LHC, many different groups and authors have discussed VBS from different points of view. Of relevance for the present work, the papers in [11] and [12] have provided new insights on both the gold-plated and the semi-leptonic decay channel as well as the determination of resonances and the coefficients of the effective lagrangian. In a parallel development, the extraction of bounds on anomalous triple and quartic gauge couplings from the LHC data was discussed in [13].

The parameterisation of the experimental results in terms of the effective chiral lagrangians was begun in [14] and further discussed in [4, 5, 15, 16]. The analysis in [17] provides an estimate of the possible limits at the LHC on the effective lagrangian coefficients—of which our work can be considered an improved and updated version.

For a more comprehensive review of the literature, the interested reader is referred to [18].

B. Notation

In this work we choose to adopt the non-linear parametrization for the EW symmetry breaking sector. This choice is particularly suitable for our purposes, since the non-linear formulation puts the longitudinal degrees of freedom of the EW gauge bosons—dominant in the VBS processes we are interested in—in foreground position.

The effective non-linear lagrangian that describes the dynamics of the Goldstone bosons associated to the $SU(2)_L \times U(1)_Y \rightarrow U(1)_{em}$ symmetry breaking pattern is organized as an expansion in powers of Goldstone bosons momenta and the number of possible operators is restricted by Lorentz, gauge, charge and parity symmetry. The leading term is of $O(p^2)$ and—in the presence of a light Higgs particle h —it can be written as

$$\mathcal{L}_0 = \frac{v^2}{4} \left[1 + 2a \frac{h}{v} + b \left(\frac{h}{v} \right)^2 \right] \text{Tr} [(D_\mu U)^\dagger (D^\mu U)] + \frac{1}{2} \partial_\mu h \partial^\mu h - V(h), \quad (1)$$

where a and b are coefficients parametrizing the Higgs interactions with the gauge bosons. The Goldstone bosons π^a ($a = 1, 2, 3$) are encoded into the matrix

$$U = \exp(i\pi^a \sigma_a / v), \quad (2)$$

where σ_a are the Pauli matrices and $v = 246$ GeV is the EW vacuum. The Goldstone matrix U has well-defined transformation properties under $SU(2)_L \times U(1)_Y$: $U \rightarrow \mathcal{G}_L U \mathcal{G}_R^\dagger$ with $\mathcal{G}_L = \exp(i\alpha^j \sigma_j / 2) \in SU(2)_L$ and $\mathcal{G}_R = \exp(i\alpha_Y \sigma_3 / 2) \in U(1)_Y$. It constitutes the building-block for the effective lagrangian with broken (non-linearly realized) EW symmetry. In eq. (1) the covariant derivative is given by

$$D_\mu U = \partial_\mu U + ig \hat{W}_\mu U - ig' U \hat{B}_\mu, \quad (3)$$

where $\hat{W}_\mu \equiv \sigma_a W_\mu^a / 2$ and $\hat{B}_\mu \equiv \sigma^3 B_\mu / 2$. The fields W_μ^a and B_μ are the $SU(2)_L \times U(1)_Y$ gauge fields with standard kinetic terms

$$\mathcal{L}_{gauge} = -\frac{1}{2} \text{Tr} \hat{W}_{\mu\nu} \hat{W}^{\mu\nu} - \frac{1}{2} \text{Tr} \hat{B}_{\mu\nu} \hat{B}^{\mu\nu}, \quad (4)$$

where $\hat{W}_{\mu\nu} = \partial_\mu \hat{W}_\nu - \partial_\nu \hat{W}_\mu + ig[\hat{W}_\mu, \hat{W}_\nu]$ and $\hat{B}_{\mu\nu} = \partial_\mu \hat{B}_\nu - \partial_\nu \hat{B}_\mu$.

In eq. (1) the quantity $V(h)$ is the Higgs boson potential with the generic structure $V(h) = \frac{1}{2} m_h^2 h^2 + d_3 (m_h^2 / 2v) h^3 + d_4 (m_h^2 / 8v^2) h^4$, where the parameters d_3 and d_4 are related to the triple and quartic Higgs self-interactions, respectively.

We extend the lagrangian in eq. (1) by adding a set of higher dimensional operators parametrizing the following $O(p^4)$ lagrangian

$$\begin{aligned} \mathcal{L}_1 = & \frac{1}{2} a_1 g g' B_{\mu\nu} \text{Tr} (T \hat{W}^{\mu\nu}) + \frac{i}{2} a_2 g' B_{\mu\nu} \text{Tr} (T [V^\mu, V^\nu]) + 2i a_3 g \text{Tr} (\hat{W}_{\mu\nu} [V^\mu, V^\nu]) \\ & + a_4 [\text{Tr} (V_\mu V_\nu)]^2 + a_5 [\text{Tr} (V_\mu V^\mu)]^2, \end{aligned} \quad (5)$$

where $V_\mu = (D_\mu U) U^\dagger$ and $T \equiv U \sigma^3 U^\dagger$. The complete list of operators entering in the chiral lagrangian at $O(p^4)$ can be found in [3]. Here we restrict to a subset of those given by eq. (5) because we are interested only in operators that modify triple and quartic gauge boson couplings and are relevant for VBS processes. In particular, the coefficient a_1 modifies the vertices with both two and three gauge bosons, a_2 and a_3 those with three gauge bosons while a_4 and a_5 only vertices with four gauge bosons. In principle, being the Higgs boson a singlet, we can add a multiplicative function of h in front of all the operators of eq. (5); a function similar to the one between squared brackets of eq. (1) but with different coefficients, as shown in [16]. Here we assume these corrections to be sub-leading and neglect them.

In the framework we have introduced, the SM corresponds to the choice $a = b = d_3 = d_4 = 1$ and $a_1 = a_2 = a_3 = a_4 = a_5 = 0$. Any departure from these values can be interpreted as presence of new physics.

C. Coefficients size and higher-order terms

The effective field theory approach to physics beyond the SM is made into an even more powerful tool after few assumptions on the ultraviolet (UV) physics are made. Without such, admittedly, speculative arguments, it remains a mere classification of effective operators without offering any particular physical insight.

The use of a non-linear realization of the electroweak symmetry naturally emerges by assuming the existence of a new strongly-interacting sector responsible for its breaking. The new sector can be characterised by two parameters: a coupling, g_* , and a mass scale, Λ . The latter identifies the mass of the heavy states populating the new sector. Furthermore—in the spirit of the non-linear σ model used in eq. (1)—it is natural to assume that the Goldstone bosons originate from the spontaneous breaking of a global symmetry of the strong sector; in this regard, the σ -model scale v is linked to the parameter of the strong sector via the relation $g_* v \approx \Lambda$. Having in mind a cut-off scale Λ of a few TeVs, the relation $g_* v \approx \Lambda$ points towards a maximally strongly coupled sector in which one expects $g_* \approx 4\pi$. In this picture the Higgs boson emerges as a light resonance of the strong sector.

The size of the effective operators generated integrating out the heavy resonances of the strong sector can be estimated by means of the so-called naïve dimensional analysis (NDA) [19]. Integrating out heavy fields at the tree level in the strong sector, the effective Lagrangian takes the following general form

$$\mathcal{L}_{\text{eff}} = \frac{\Lambda^4}{g_*^2} \hat{\mathcal{L}} \left[\frac{\partial_\mu}{\Lambda}, \frac{g_* h}{\Lambda}, \frac{g_* \pi^a}{\Lambda}, \frac{g A_\mu}{\Lambda}, \frac{g A_{\mu\nu}}{\Lambda^2} \right], \quad (6)$$

where A_μ ($A_{\mu\nu}$) denotes a generic gauge field (field strength) while $\hat{\mathcal{L}}$ is a dimensionless functional. For simplicity, we neglect fermionic contributions since they are not important in our setup. The most relevant information in eq. (6) is

that the Goldstone bosons and the Higgs are always accompanied by an insertion of g_* since they are directly coupled to the strong sector they belong to.

We can now analyze by power counting the effective operators, written in eq. (5), relevant for the WW scattering process we are interested in:

- The effective operators $a_4 [\text{Tr}(V_\mu V_\nu)]^2$ and $a_5 [\text{Tr}(V_\mu V^\mu)]^2$ generate the quadrilinear vertex involving four Goldstone boson derivatives. Using the rules of NDA we find the corresponding WW scattering amplitude to be proportional to $g_*^2(E/\Lambda)^4$, where E is the characteristic center-of-mass energy of the process (for the sake of simplicity we do not distinguish here between different WW channels, since we are simply interested in an order-of-magnitude estimate of the amplitude);

- The operator $a_3 \text{Tr}(\hat{W}_{\mu\nu}[V^\mu, V^\nu])$ generates the trilinear coupling

$$\epsilon_{kAB}(\partial_\mu W_\nu^k - \partial_\nu W_\mu^k)(\partial^\mu \pi^A \partial^\nu \pi^B - \partial^\nu \pi^A \partial^\mu \pi^B). \quad (7)$$

The corresponding WW scattering amplitude involves the s -, t -, and u -channel exchange of the EW gauge bosons $W^{k=1,2,3}$, and from NDA we obtain an amplitude proportional to $g^2(E/\Lambda)^4$;

- The operator $a_2 B_{\mu\nu} \text{Tr}(T[V^\mu, V^\nu])$ generates the trilinear coupling

$$\epsilon_{3AB}(\partial_\mu B_\nu - \partial_\nu B_\mu)(\partial^\mu \pi^A \partial^\nu \pi^B - \partial^\nu \pi^A \partial^\mu \pi^B). \quad (8)$$

The corresponding WW scattering amplitude involves the s -, t -, and u -channel exchange of the EW gauge boson B , and from NDA we obtain an amplitude proportional to $g'^2(E/\Lambda)^4$;

- Finally, the σ -model operator $\text{Tr}[(D_\mu U)^\dagger(D^\mu U)]$ generates the trilinear structures

$$\epsilon_{kAB} W_\mu^k [(\partial^\mu \pi^A) \pi^B - (\partial^\mu \pi^B) \pi^A] \quad \text{and} \quad \epsilon_{3AB} B_\mu [(\partial^\mu \pi^A) \pi^B - (\partial^\mu \pi^B) \pi^A]. \quad (9)$$

By combining these vertices with the trilinear interactions extracted before from $a_3 \text{Tr}(\hat{W}_{\mu\nu}[V^\mu, V^\nu])$ and $a_2 B_{\mu\nu} \text{Tr}(T[V^\mu, V^\nu])$, we find an amplitude proportional to, respectively, $g^2(E/\Lambda)^2$ and $g'^2(E/\Lambda)^2$.

Notice that the energy dependence of these amplitudes—obtained here by dimensional analysis—will be confirmed by means of a direct computation in section II D.

We can now compare the amplitude proportional to $a_{4,5}$ against that proportional to a_2 . Both these amplitudes grow with E^4 ; however, the contribution coming from the operators $a_4 [\text{Tr}(V_\mu V_\nu)]^2$ and $a_5 [\text{Tr}(V_\mu V^\mu)]^2$ is parametrically enhanced since proportional to g_*^2 . Similarly, we can compare the same amplitude against that proportional to a_3 . The former dominates if the condition $g_*(E/\Lambda) > g$ is satisfied. Since $g_* v \approx \Lambda$, it implies $E > gv$, a condition easily satisfied at typical LHC energies.

It therefore seems natural to expect that in the presence of a genuinely strongly coupled new sector the most relevant contribution to the WW scattering arises from the pure Goldstone operators $a_4 [\text{Tr}(V_\mu V_\nu)]^2$ and $a_5 [\text{Tr}(V_\mu V^\mu)]^2$. For this reason in section II we will focus our Monte Carlo analysis on the two coefficients a_4 and a_5 , setting $a_2 = a_3 = 0$.

Finally, notice that the same NDA argument can be used in order to estimate the contribution of $O(p^6)$ (or higher) operators. For definiteness, let us consider the $O(p^6)$ operator $\epsilon_{ABC}(W^A)_\mu^\nu(W^B)_{\nu\rho}(W^C)^{\rho\mu}$. It generates the quadrilinear vertex

$$\epsilon_{ABC}\epsilon_{AB'C'}(\partial_\mu W^{B,\nu} - \partial^\nu W_\mu^B)(\partial_\nu W_\rho^C - \partial_\rho W_\nu^C)W^{B',\rho}W^{C',\mu} \quad (10)$$

which contributes to the WW (transverse) scattering according to $g^2(g^2/g_*^2)(E/\Lambda)^2$.¹ As evident from the previous discussion, the maximally strongly coupled limit $g_* \approx 4\pi$ suppresses this contribution that in principle could interfere with the perturbative expansion.

¹ A further loop-suppression $g_*/(4\pi)^2$ is expected, since this operator can not be generated by integrating out at the tree level any resonance with spin less than 2. However, since we have in mind the limit $g_* \approx 4\pi$, the presence of this extra factor does not change our estimate.

D. Mapping to other formulations

It is useful to map the non-linear formalism into other popular parameterizations—thus providing a dictionary through which to translate all the available bounds. In the following, we briefly discuss the relations with *i*) the phenomenological lagrangian commonly used to parametrize triple and quartic anomalous gauge boson couplings and *ii*) the higher dimensional effective lagrangian obtained by imposing the additional assumption that the Higgs field h is part of a $SU(2)_L$ doublet that breaks the EW symmetry.

1. Anomalous triple and quartic gauge couplings

Traditionally bounds on triple gauge boson couplings (TGC) have been expressed in terms of anomalous coefficients [22], according to the following phenomenological lagrangian

$$\begin{aligned} \mathcal{L}_{\text{TGC}} = & ie \left[g_1^\gamma A_\mu (W_\nu^- W^{+\mu\nu} - W_\nu^+ W^{-\mu\nu}) + \kappa^\gamma W_\mu^- W_\nu^+ A^{\mu\nu} + \frac{\lambda^\gamma}{m_W^2} W_\mu^{-\nu} W_{\nu\rho}^+ A^{\rho\mu} \right] \\ & + \frac{ie c_W}{s_W} \left[g_1^Z Z_\mu (W_\nu^- W^{+\mu\nu} - W_\nu^+ W^{-\mu\nu}) + \kappa^Z W_\mu^- W_\nu^+ Z^{\mu\nu} + \frac{\lambda^Z}{m_W^2} W_\mu^{-\nu} W_{\nu\rho}^+ Z^{\rho\mu} \right], \end{aligned} \quad (11)$$

where $W_{\mu\nu}^\pm \equiv \partial_\mu W_\nu^\pm - \partial_\nu W_\mu^\pm$, $V_{\mu\nu} \equiv \partial_\mu V_\nu - \partial_\nu V_\mu$, with $V = A, Z$. The SM corresponds to $g_1^{\gamma,Z} = \kappa^{\gamma,Z} = 1$, $\lambda^{\gamma,Z} = 0$.

In our case κ_Z , κ_γ and g_1^Z (g_1^γ is fixed to be 1 by gauge invariance) are modified by the presence of the operators in eq. (5). By inspection, we can identify the following identities:

$$\Delta g_1^Z = \frac{g'^2}{c_W^2 - s_W^2} a_1 + \frac{2g^2}{c_W^2} a_3, \quad \Delta \kappa^\gamma = g^2(a_2 - a_1) + 2g^2 a_3, \quad \Delta \kappa^Z = \frac{g'^2}{c_W^2 - s_W^2} a_1 - g'^2(a_2 - a_1) + 2g^2 a_3. \quad (12)$$

Furthermore, it follows that $\Delta \kappa^Z = \Delta g_1^Z - (g'^2/g^2)\Delta \kappa^\gamma$. For illustrative purposes we can take $a_1 = 0$, as suggested by the stringent fit of LEP data of [27]. In this case the previous relations simplify to

$$\Delta g_1^Z = \frac{2g^2}{c_W^2} a_3, \quad \Delta \kappa^\gamma - \Delta \kappa^Z = (g^2 + g'^2) a_2. \quad (13)$$

As far as the anomalous quartic gauge couplings (QGC) are concerned, they are usually parametrized as follows

$$\begin{aligned} \mathcal{L}_{\text{QGC}} = & e^2 g_{WWVV} [g_1^{VV} V^\mu V^\nu W_\mu^- W_\nu^+ - g_2^{VV} V^\mu V_\mu W^{-\nu} W_\nu^+] \\ & + \frac{e^2 c_W}{s_W} \left[g_1^{\gamma Z} A^\mu Z^\nu (W_\mu^- W_\nu^+ + W_\mu^+ W_\nu^-) - 2g_2^{\gamma Z} A^\mu Z_\mu W^{-\nu} W_\nu^+ \right] \\ & + \frac{e^2}{2s_W^2} [g_1^{WW} W^{-\mu} W^{+\nu} W_\mu^- W_\nu^+ - g_2^{WW} (W^{-\mu} W_\mu^+)^2] + \frac{e^2}{4s_W^2 c_W^4} h^{ZZ} (Z_\mu Z^\mu)^2, \end{aligned} \quad (14)$$

with $g_{WW\gamma\gamma} = 1$, $g_{WWZZ} = c_W^2/s_W^2$. The SM corresponds to $g_{1/2}^{VV'} = 1$, $h^{ZZ} = 0$. The effective operators of eq. (5) produce the following corrections

$$\Delta g_1^{\gamma Z} = \Delta g_2^{\gamma Z} = \frac{g'^2}{c_W^2 - s_W^2} a_1 + \frac{2g^2}{c_W^2} a_3, \quad \Delta g_2^{ZZ} = 2\Delta g_1^{\gamma Z} - \frac{g^2}{c_W^4} a_5, \quad (15)$$

$$\Delta g_1^{ZZ} = 2\Delta g_1^{\gamma Z} + \frac{g^2}{c_W^4} a_4, \quad \Delta g_1^{WW} = 2c_W^2 \Delta g_1^{\gamma Z} + g^2 a_4, \quad (16)$$

$$h^{ZZ} = g^2(a_4 + a_5), \quad \Delta g_2^{WW} = 2c_W^2 \Delta g_1^{\gamma Z} - g^2(a_4 + 2a_5). \quad (17)$$

2. Comparison with the linear realization

At dimension 6, the bosonic operators relevant for our discussion are [23]

$$\begin{aligned}
\mathcal{O}_{WB} &= \frac{g\kappa_{WB}}{4m_W^2} B^{\mu\nu} W_{\mu\nu}^k H^\dagger \sigma^k H, & \mathcal{O}_{3W} &= \frac{g\kappa_{3W}}{6m_W^2} \epsilon^{ijk} W_{\mu\nu}^i W_\rho^{j\nu} W^{k\rho\mu}, & \mathcal{O}_H &= \frac{\kappa_H}{v^2} \partial^\mu (H^\dagger H) \partial_\mu (H^\dagger H), \\
\mathcal{O}_{HW} &= \frac{ig\kappa_{HW}}{m_W^2} (D^\mu H)^\dagger \sigma^k (D^\nu H) W_{\mu\nu}^k, & \mathcal{O}_W &= \frac{ig\kappa_W}{2m_W^2} H^\dagger \sigma^k \overleftrightarrow{D}_\mu H (D_\nu W^{k\mu\nu}), & \mathcal{O}_{WW} &= \frac{g^2\kappa_{WW}}{4m_W^2} (H^\dagger H) W_{\mu\nu}^k W^{k\mu\nu}, \\
\mathcal{O}_{HB} &= \frac{ig'\kappa_{HB}}{m_W^2} (D_\mu H)^\dagger (D_\nu H) B^{\mu\nu}, & \mathcal{O}_B &= \frac{ig'\kappa_B}{2m_W^2} H^\dagger \overleftrightarrow{D}_\mu H (\partial_\nu B^{\mu\nu}), & \mathcal{O}_{BB} &= \frac{g'^2\kappa_{BB}}{4m_W^2} (H^\dagger H) B_{\mu\nu} B^{\mu\nu}, \\
\mathcal{O}_{2W} &= \frac{g^2\kappa_{2W}}{16m_W^2} (D_\rho W_{\mu\nu}^k)^2, & \mathcal{O}_{2B} &= \frac{g'^2\kappa_{2B}}{16m_W^2} (D_\rho B_{\mu\nu})^2, & &
\end{aligned} \tag{18}$$

with $H^\dagger \overleftrightarrow{D}_\mu H = H^\dagger (D_\mu H) - (D_\mu H)^\dagger H$. H is the Higgs doublet of the SM with hypercharge $Y_H = 1/2$. The operators $\mathcal{O}_{H,WW,BB}$ in the last column affect only Higgs physics while the remaining ones affect the electroweak precision observables. Three operators \mathcal{O}_{3W} , \mathcal{O}_{WW} and \mathcal{O}_W enter in WW vector boson scattering.

Notice that there is a redundancy in this list, since it is possible to remove some of these operators using the equation of motion of the gauge fields and the operator identities $\mathcal{O}_{HB} = \mathcal{O}_B - \mathcal{O}_{WB} - \mathcal{O}_{BB}$, and $\mathcal{O}_{HW} = \mathcal{O}_W - \mathcal{O}_{WB} - \mathcal{O}_{WW}$.² For instance in the SILH basis used in [24] the operators $\mathcal{O}_{2W,2B,WB,WW}$ are dropped while in the so-called Warsaw basis [25] the operators $\mathcal{O}_{2W,2B,WB,HW,HB}$ are dropped. By comparing the anomalous TGC, we find

$$\Delta g_1^Z = g^2 \left(\frac{s_W^2}{c_W^2 - s_W^2} a_1 + \frac{2a_3}{c_W^2} \right) = \kappa_W + \kappa_{HW}, \quad \Delta \kappa^\gamma = g^2 (a_2 - a_1 + 2a_3) = -\kappa_{WB} + \kappa_{HW} + \kappa_{HB}. \tag{19}$$

There are 18 operators of dimension 8 but only two

$$\mathcal{O}_{S,0} = \frac{f_{S,0}}{\Lambda^4} [(D_\mu H)^\dagger D_\nu H] [(D^\mu H)^\dagger D^\nu H], \quad \mathcal{O}_{S,1} = \frac{f_{S,1}}{\Lambda^4} [(D_\mu H)^\dagger D^\mu H] [(D^\nu H)^\dagger D_\nu H], \tag{20}$$

are relevant for us. The other 16 operators of dimension 8—five of which enter WW scattering—have derivative terms in the vector bosons in addition to those with the Higgs field, and would have to be matched to higher order terms in the chiral lagrangian. For the WW channel we are interested in, we find [26]:

$$a_4 = \frac{f_{S,0}}{\Lambda^4} \frac{v^4}{8}, \quad \text{and} \quad a_4 + 2a_5 = \frac{f_{S,1}}{\Lambda^4} \frac{v^4}{8}. \tag{21}$$

E. Current and estimated bounds

Current bounds on the coefficients of the operators in eq. (5) come from EW precision measurements performed at LEP-I and LEP-II and from data collected at LHC run 1. Estimated bounds are meant to be for LHC run 2.

1. Electroweak precision tests

The coefficient a_1 is strongly constrained by LEP-I and LEP-II data because it contributes at tree-level to the S parameter

$$\Delta S = -16\pi a_1. \tag{22}$$

A simple fit of LEP data [27] performed including the correction in eq. (22) shows that

$$a_1 = (1.0 \pm 0.7) \times 10^{-3}. \tag{23}$$

² In [26] (using the notation of eq. (18)) the subset $\{\mathcal{O}_H, \mathcal{O}_{3W}, \mathcal{O}_{HW}, \mathcal{O}_{HB}, \mathcal{O}_{WW}, \mathcal{O}_{BB}\}$ was considered.

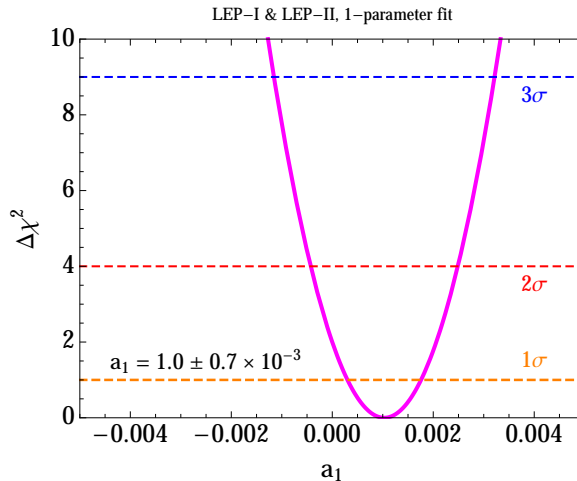


FIG. 1: $\Delta\chi^2$ plot for the limit on the coefficient a_1 from LEP I and II precision tests.

On the other hand, the other coefficients a_2 , a_3 , a_4 and a_5 contribute to the S, T, U parameters only at at one-loop. In particular, the one-loop contributions of a_4 and a_5 to EW precision measurements lead to the following (rather weak) bounds on these coefficients at 90% CL [16]

$$-0.094 < a_4 < 0.10 \quad \text{and} \quad -0.23 < a_5 < 0.26. \quad (24)$$

The combined LEP bounds on TGC [28] are

$$-0.054 < \Delta g_1^Z < 0.021 \quad -0.07 < \Delta\kappa_Z < 0.051 \quad -0.099 < \Delta\kappa_\gamma < 0.066 \quad (95\% \text{ CL}). \quad (25)$$

By means of the relations in eq. (13) we can translate the above bounds into limits on the coefficients a_2 and a_3

$$-0.26 < a_2 < 0.26 \quad \text{and} \quad -0.10 < a_3 < 0.04, \quad (26)$$

which are in agreement with the ones found in [16].

2. LHC run 1 and run 2

Current experimental limits on a_4 and a_5 based on LHC run 1 are still rather weak and comparable to those in eq. (24) coming from EW precision measurements. ATLAS and CMS find [30]

$$-0.14 < a_4 < 0.16 \quad \text{and} \quad -0.23 < a_5 < 0.24 \quad (27)$$

at the 95% CL and with a luminosity of 20.3 fb^{-1} (CM energy of 8 TeV). These bounds are obtained by studying the double charged channel (after unitarization by means of the K -matrix method).

Estimated bounds on a_4 at the LHC run 2 presented in [31] represent a substantial improvement with respect to the current LHC limits, namely

$$a_4 \leq 0.066. \quad (28)$$

This limit is obtained at 95% CL and for a luminosity of 300 fb^{-1} (CM energy of 14 TeV).

The best existing estimated limit is obtained in [17] where they combine same- and opposite-sign channels. They find

$$-22 < \frac{f_0}{\Lambda^4} (\text{TeV}^{-4}) < 24 \quad \text{and} \quad -25 < \frac{f_1}{\Lambda^4} (\text{TeV}^{-4}) < 25 \quad (29)$$

at the 99% CL and for a luminosity of 100 fb^{-1} (CM energy of 14 TeV). These bounds are equivalent by means of eq. (21) to

$$-0.01 < a_4 < 0.01 \quad \text{and} \quad -0.01 < a_5 < 0.01. \quad (30)$$

Recent data on the Higgs boson decays indicate a value for the Higgs coupling to the gauge bosons very close to the SM value, namely [32]

$$a = 1.03 \pm 0.06. \quad (31)$$

No dramatic improvement on this limit is expected from future LHC runs due to systematic errors [33].

3. Analyticity and causality

The causal and analytic structure of the amplitudes leads to theoretical bounds on the possible values the two coefficients a_4 and a_5 can assume [15, 29]. The most stringent of these comes from the requirement that the underlying theory respects causality:

$$a_4(\mu) \geq \frac{1}{12} \frac{1}{(4\pi)^2} \log \frac{\Lambda^2}{\mu^2} \quad \text{and} \quad a_4(\mu) + a_5(\mu) \geq \frac{1}{8} \frac{1}{(4\pi)^2} \log \frac{\Lambda^2}{\mu^2}, \quad (32)$$

where Λ represents the cutoff of the effective theory and $\mu < \Lambda$ the scale at which the amplitude is evaluated. For most practical purposes, we can neglect the logarithms and take

$$a_4 > 0 \quad \text{and} \quad a_4 + a_5 > 0 \quad (33)$$

as our causality bounds. In our limits, we will assume them to be satisfied. Even though a violation of the above constraints would imply a (hard to entertain) breach in the causal structure of the theory, it is useful to bear in mind that this possibility cannot be ruled out *a priori* and that an observation of a negative value of a_4 or of the combination $a_4 + a_5$ would be a really striking discovery in as much as it would challenge the very foundations of quantum field theory.

II. METHODS

In section II A we present some details about the Monte Carlo simulation we have implemented in order to generate the VBS processes we are interested in. In section II B we describe the selection cuts we have employed. The statistical framework and the estimation of the effects of systematic errors are presented in section II C. Finally, in section II D we discuss the violation of unitarity that can potentially arise and explain the unitarization procedure we have applied.

A. Monte Carlo simulation

We have modeled the effective lagrangian consisting of the sum of the terms in eq. (1), (4) and (5) by means of FEYNRULES [34] v2.0.28 in order to create the UFO module that is used in MADGRAPH5 [35] v2.2.3 to simulate signal and background events related to the VBS processes we are interested in.

Pure EW same-sign (SS) WW events in $pp \rightarrow W^\pm W^\pm jj \rightarrow l^\pm \nu_l l^\pm \nu_l jj$ and EW opposite-sign (OS) WW events in $pp \rightarrow W^\pm W^\mp jj \rightarrow l^\pm \nu_l l^\mp \nu_l jj$ are $O(\alpha_W^6)$. Mixed QCD/EW SS and OS WW events are $O(\alpha_W^4 \alpha_s^2)$.

The relevant diagrams for probing the symmetry breaking dynamics must contain direct W boson interactions. They are only a small fraction of the whole set in pure EW events—which are dominated by diagrams in which the W bosons are radiated from the incoming quarks, do not interact and have predominantly a transverse polarisation. Mixed QCD/EW events—in which the vector bosons are produced from strongly scattered quarks—only contain diagrams in which the W bosons do not interact. These two processes constitute the main irreducible background for our analysis.

Other background processes that contribute to SS and OS WW channels are the following:

- Z +jets: events from this process can easily enter the OS channel and even the SS channel if the sign of one lepton is mis-identified;
- $t\bar{t}$: the same considerations apply as for Z +jets, but this kind of events are expected to be harder to suppress due to the higher probability of having more energetic jet and lepton pairs with large angular separation (and therefore higher invariant masses);

- WZ +jets, $t\bar{t}W$, $t\bar{t}Z$ and $t\bar{t}H$: events from these processes can originate high energy jets together with two or more charged leptons, which can even enter the SS leptons selection, in case of three or more leptons or one lepton from the $t\bar{t}$ decay and another one from the associated boson decay;
- single-lepton+jet (*e.g.* from W +jets): these events can enter any of the two channels if a jet is mis-identified as an additional isolated lepton.

Among the processes listed above, we have included the WZ +jets background in the study of the SS channel and the $t\bar{t}$ background in that of the OS channel. The other processes are highly suppressed by the selection cuts, resulting in negligible effects in the analysis. We are, however, aware that this suppression depends on our Monte Carlo simulation which does not predict correctly the effects of lepton charge mis-identification and jets reconstructed as leptons in the detector.

The simulated events have been showered using `Pythia 6.4` [36] and subsequently processed through `Delphes` [37] in order to simulate the response of a generic LHC detector. All the settings for both `Pythia` and `Delphes` have been kept as default (*i.e.*, leaving the default options when installing the software through the `Madgraph5` interface).

The number of events from each process has been then rescaled according to the LO cross-section and the expected integrated luminosity in each of the considered cases, to obtain an expected yield after the event selection.

B. Selection cuts

As already discussed, the pure EW production of WW pairs in association with two jets at the LHC is dominated by events that have no direct relevance for the mechanism of electroweak symmetry breaking. Typically these events come from soft collisions involving incoming partons which lead to soft accompanying parton jets in the final state and can be rejected by appropriate cuts on their rapidity. In order to suppress this irreducible background and select events with hard WW interactions we apply the following selection criteria

- small pseudo-rapidity and large transverse momentum for the W gauge bosons;
- two opposite tagging jets at large pseudo-rapidities and relatively small transverse momentum.

Beside reducing the irreducible EW background, these cuts also suppress the mixed EW/QCD one.

Subsequently we have to impose additional cuts in order to wean out the transversally polarised vector bosons—which accounts for more than 90% of the total produced W pairs—and select the longitudinally polarised ones. At the parton level, the production of longitudinally polarised W is characterised by the final quark which is emitted more forward than in the case of the production of transversally polarised W . Moreover, after being produced by bremsstrahlung, the W_L (mostly) conserve their polarisation—as long as we stay above the on-shell production threshold.

The complete set of cuts applied in the case of SS and OS WW channels are summarized below.

1. Same-sign WW channel

We select events by applying the following set of cuts:

- two same-sign leptons with $p_T^{l\pm} > 20$ GeV and $|\eta_{l\pm}| < 2.5$;
- at least two jets ($p_T^j > 25$ GeV and $|\eta_j| < 4.5$) with relative rapidity $|\Delta y_{jj}| > 2.4$;
- the two highest p_T jets with an invariant mass $m_{jj} > 500$ GeV;
- missing transverse energy $E_T^{miss} > 25$ GeV.

This combined set of cuts has been optimized for VBS at the energy of 14 TeV, condering an integrated luminosity of 300 fb^{-1} and are rather close to those already in use by the LHC experimental collaborations.

The cuts above only partially succeed in singling out the longitudinal W bosons and a rather large pollution from the transversally polarized ones is still present. To improve further the selection efficiency of the longitudinal modes we add the Warsaw cut [6] defined as follows

$$R_{p_T} = \frac{p_T^{l_1} p_T^{l_2}}{p_T^{j_1} p_T^{j_2}} > 3.5. \quad (34)$$

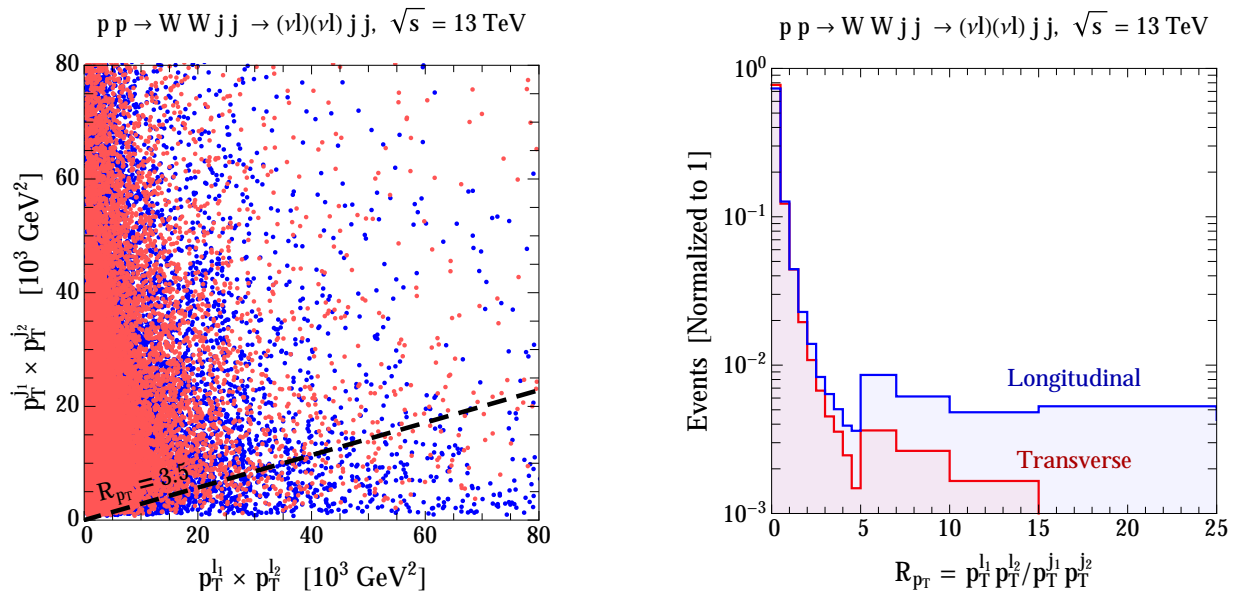


FIG. 2: Distribution of final state events obtained generating the processes $pp \rightarrow W^\pm W^\pm jj \rightarrow (l^\pm \nu_l)(l^\pm \nu_l) jj$ at the LHC with $\sqrt{s} = 13$ TeV. We show in blue (red) the events with leptons coming from the decay of longitudinal (transverse) polarized W bosons.

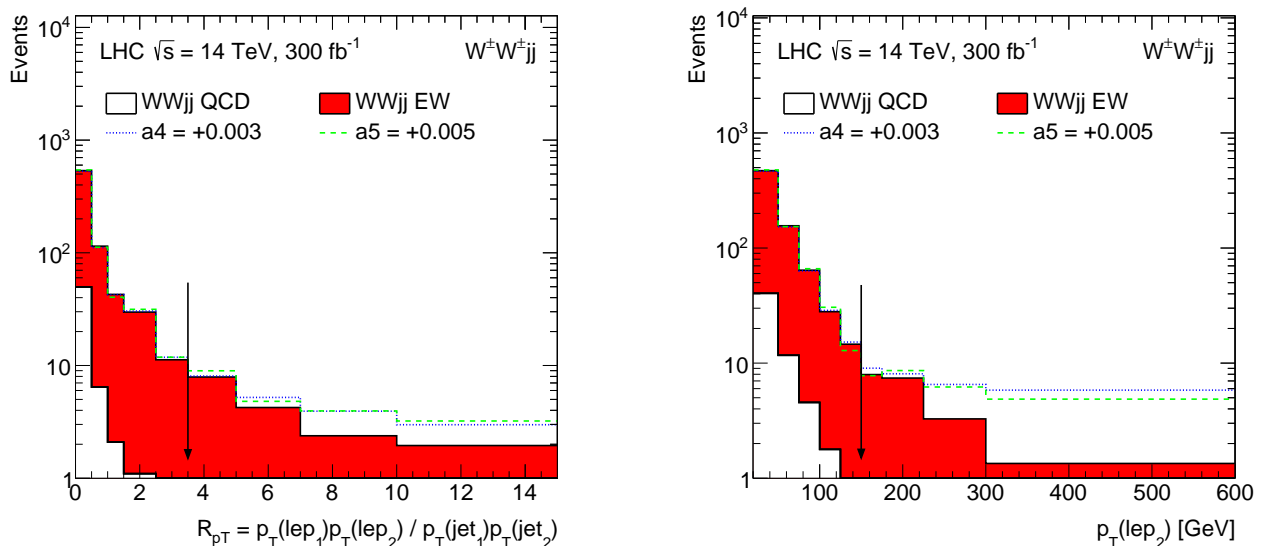


FIG. 3: Comparison of selection cuts: $R_{p_T} > 3.5$ vs. $p_T^{lep} > 150$ GeV. In red (white) the EW (QCD) contribution. The dashed lines mark the number of events in the presence of non-vanishing coefficients of the effective lagrangian ($a_4 = 0.003$ and $a_5 = 0.005$)

The R_{p_T} variable contains the information about the momenta of the final leptons and is very effective in separating the transverse from the longitudinal modes.

The discriminating power of this cut is illustrated in the left plot of Fig. 2. The red (blue) points represent the distribution in the $[p_T^{l1} p_T^{l2}, p_T^{j1} p_T^{j2}]$ plane of $pp \rightarrow W^\pm W^\pm jj \rightarrow l^\pm \nu_l l^\pm \nu_l jj$ events at the LHC ($\sqrt{s} = 13$ TeV) containing transverse (longitudinally) polarized WW pairs. By inspection we see that the cut $R_{p_T} > 3.5$ is very useful in discriminating longitudinal from transverse polarized W bosons. The power of this selection is even more evident from the histogram shown in the right panel of Fig 2, where the same distribution of events is plotted as a function of the ratio R_{p_T} .

TABLE I: Comparison of upper exclusion limits (at 95% and 99% CL) and discovery significance (at 3 and 5 σ) for the effective lagrangian coefficients a_4 and a_5 , for CM energy $\sqrt{s} = 14$ TeV and luminosity 300 fb^{-1} , using the selection cut on R_{p_T} and p_T . Values for both coefficients obtained by only using the same-sign WW channel.

$\sqrt{s} = 14 \text{ TeV}, 300 \text{ fb}^{-1}$				
$R_{p_T} > 3.5$			$p_T^{lep} > 150 \text{ GeV}$	
	95% (99%)	3 σ (5 σ)	95% (99%)	3 σ (5 σ)
a_4	0.0027 (0.0034)	0.0032 (0.0041)	0.0031 (0.0038)	0.0036 (0.0047)
a_5	0.0055 (0.0068)	0.0064 (0.0084)	0.0063 (0.0078)	0.0074 (0.0097)

In [17] the selection on the W polarisation is carried out by means of a selection on the lepton momentum instead of the Warsaw cut. Fig. 3 compares the two choices and Table V shows the upper limits for the coefficients of the effective lagrangian obtained by means of the two possible selection cuts. We find the Warsaw cut to be better in weaning out the transverse polarizations. In any case, the similarity in the selection choice is reflected in our final limits that turn out to be rather close to those of [17] for comparable energies and luminosities.

Table II shows the effect of the various selection cuts on the number of surviving events in the SS channel. Fig. 4 shows the position of the cut selection for the variables Δy_{jj} , m_{jj} and R_{p_T} for this channel.

TABLE II: Cutflow (number of events for each process cut by cut) for the SS channel for CM energy $\sqrt{s} = 14$ TeV and luminosity 300 fb^{-1} .

$\sqrt{s} = 14 \text{ TeV}, 300 \text{ fb}^{-1}$				
cut	WZjj	WWjj QCD	WWjj EW	S ($a_4 = 0.02$)
2 SS leptons	4474	778	1343	1289
$E_T^{miss} > 25 \text{ GeV}$	3705	703	1225	1262
$\Delta y_{jj} > 2.4$	536	181	746	900
$m_{jj} > 500 \text{ GeV}$	330	60	678	890
$R_{p_T} > 3.5$	6.5	0.5	17	747

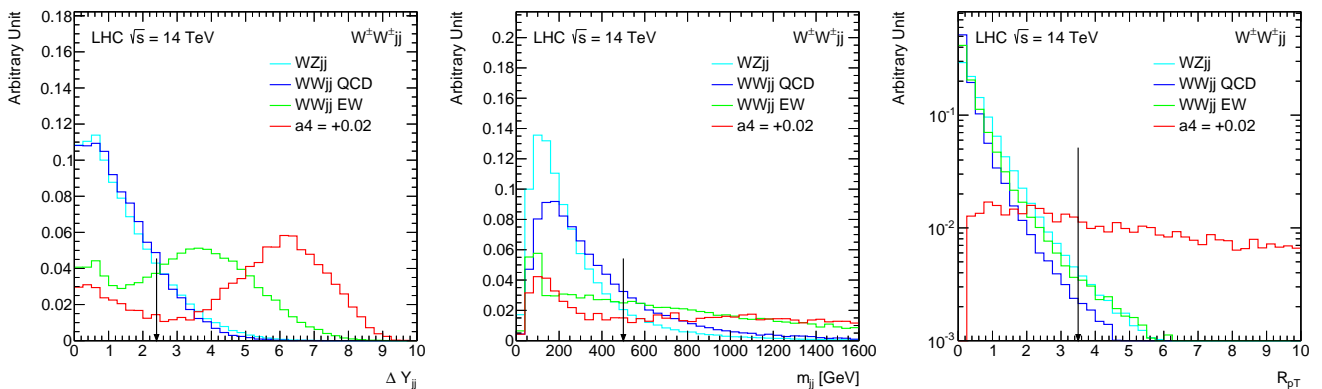


FIG. 4: Position of the cut selection for the three variables Δy_{jj} , m_{jj} and R_{p_T} in the SS channel.

TABLE III: Cutflow (number of events for each process cut by cut) for the OS channel for CM energy $\sqrt{s} = 14$ TeV and luminosity 300 fb^{-1} .

$\sqrt{s} = 14 \text{ TeV}, 300 \text{ fb}^{-1}$				
cut	$t\bar{t}$	$WWjj$ QCD	$WWjj$ EW	S ($a_5 = 0.02$)
2 OS leptons	1975270	68884	3221	498
$E_T^{miss} > 25 \text{ GeV}$	1791100	61494	2927	488
$m_{jj} > 500 \text{ GeV}$	109885	6761	1569	380
$\Delta y_{jj} > 2.4$	78144	4543	1369	394
$R_{p_T} > 3.5$	1461	114	44	287
$m_T^{WW} > 800 \text{ GeV}$	504	40	19	231
$\Delta\Phi_{\ell\ell} > 2.25$	453	34	19	231
b -tag veto	353	34	19	227
N jets < 3	21	14	11	148

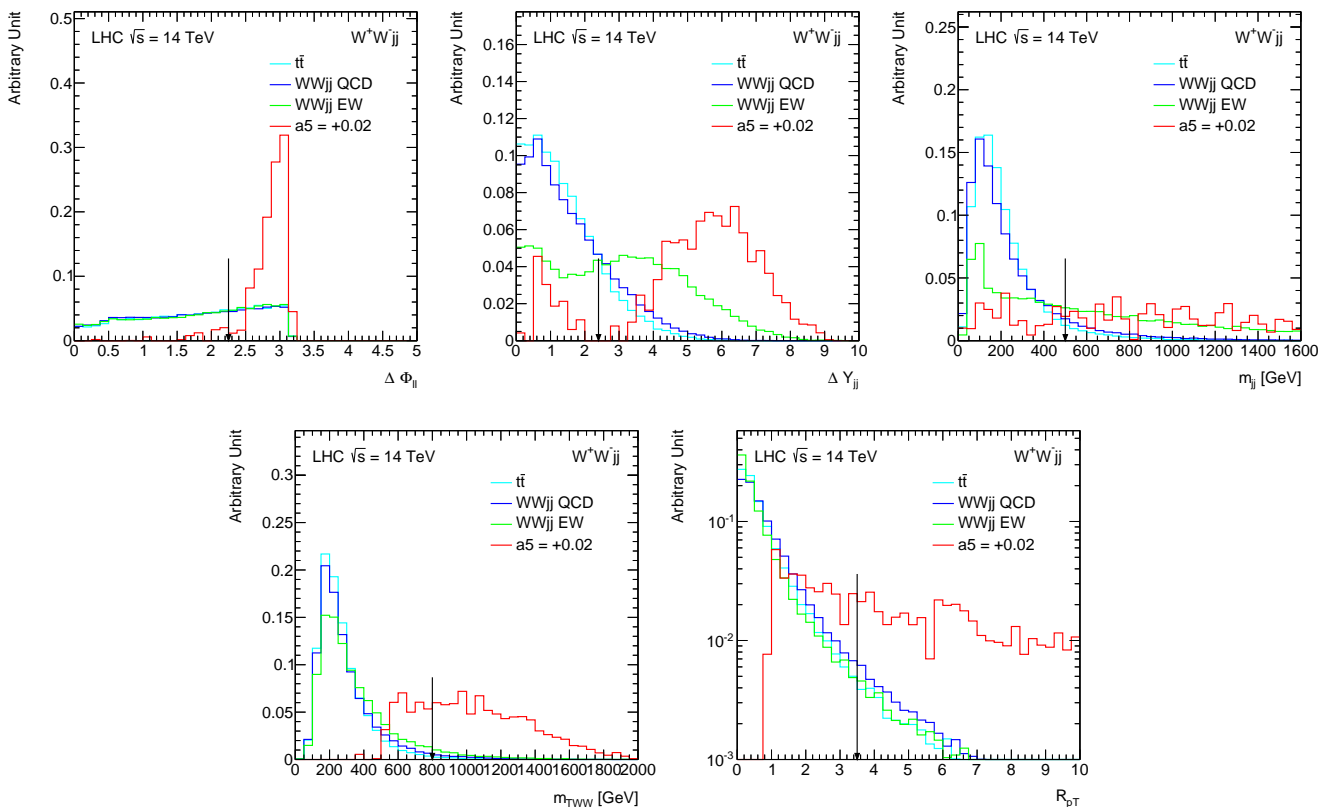


FIG. 5: Position of the cut selection for the three variables $\Delta\Phi_{\ell\ell}$, Δy_{jj} , m_{jj} , m_T^{WW} and R_{p_T} in the OS channel.

2. Opposite-sign WW channel

The opposite-sign decay channel is less clean because of the large reducible background coming from $t\bar{t}$ pair production. For this channel in the process $pp \rightarrow l^\pm \nu_l l^\mp \nu_l jj$ we use the following selection cuts:

- two opposite-sign leptons with $p_T^{l^\pm} > 20 \text{ GeV}$ and $|\eta_{l^\pm}| < 2.5$;

- missing transverse energy $E_T^{miss} > 25$ GeV
- the two highest p_T jets with an invariant mass $m_{jj} > 500$ GeV;
- two and only two jets ($p_T^j > 25$ GeV and $|\eta_j| < 4.5$) with relative rapidity $|\Delta y_{jj}| > 2.4$;
- $R_{p_T} > 3.5$;
- invariant transverse mass $m_T^{WW} > 800$ GeV;
- angular separation between the leptons in the transverse plane $|\Delta\Phi_{ll}| > 2.25$;
- b -quark veto (*i.e.* no jets tagged by the b -tagging algorithm implemented in **Delphes**).

The invariant transverse mass in the cuts above is defined as

$$m_T^{WW} = \sqrt{\left(\sqrt{(p_T^l)^2 + m_{ll}^2} + \sqrt{(E_T^{miss})^2 + m_{ll}^2}\right)^2 - (\vec{p}_T^{ll} + \vec{p}_T^{miss})^2}, \quad (35)$$

where \vec{p}_T^{miss} is the missing transverse momentum vector, \vec{p}_T^{ll} is the transverse momentum of the di-lepton pair and m_{ll} its mass.

Table III shows the effect of the various selection cuts on the number of surviving events in OS channel. Fig. 5 shows the position of the cut selection for the variables $\Delta\Phi_{\ell\ell}$, Δy_{jj} , m_{jj} , $m_{\ell\ell}$ and R_{p_T} for this channel.

C. Statistical analysis

In the following we will compute the expected discovery significance and the expected exclusion limits for the coefficients of the effective lagrangian in eq. (1) and eq. (5).

For a given set of selection cuts, we define the signal S as the enhancement in the number of $WWjj$ events—obtained for certain fixed values of the coefficients a , a_2 , a_3 , a_4 and a_5 —over the SM prediction (obtained for $a = 1$, $a_2 = a_3 = a_4 = a_5 = 0$)

$$S = \mathcal{N}_{ev}(pp \rightarrow WWjj) \Big|_{a, a_2, a_3, a_4, a_5} - \mathcal{N}_{ev}(pp \rightarrow WWjj) \Big|_{a=1, a_2=a_3=a_4=a_5=0}. \quad (36)$$

The background B is given by the number of events predicted by the SM

$$B = \mathcal{N}_{ev}(pp \rightarrow WWjj) \Big|_{a=1, a_2=a_3=a_4=a_5=0} + \mathcal{N}_{ev}(pp \rightarrow t\bar{t}/WZjj) \Big|_{a=1, a_2=a_3=a_4=a_5=0}. \quad (37)$$

The expected number of signal events S is compared with the number of background events B using Poisson statistics without considering any systematic uncertainty. The Poisson probability density function is generalized to non-integer event numbers through the use of the Gamma function.

1. Discovery significance and exclusion limits

For each set of values of the effective couplings, the expected discovery significance is obtained by computing the probability of observing a number of events greater or equal to $S + B$ assuming the background-only hypothesis. This probability is then translated into a number of Gaussian standard deviations: three (five) standard deviations is considered as benchmark for an observation (discovery). On the other hand, the expected exclusion limits are obtained by computing the probability of observing a number of events less or equal to B assuming the signal-plus-background hypothesis. The specific choice of the parameters is considered excluded at 95% (99%) CL if this probability is less or equal than 5% (1%).

Notice that, for large values of B , the Poisson distribution can be very well approximated by a Gaussian function. In this case the significance (expressed in terms of number of standard deviations) can be computed simply as S/\sqrt{B} . In the same limit we can say that a set of parameters is excluded at 95% (99%) CL if the quantity $S/\sqrt{S+B} > 2$ (> 3).

The difference between using the exact Poisson distribution and the approximated formulas above can be gauged in Fig. 6 where the χ^2 test is run for the two possibilities. As one can see by inspection, while for the case at $\sqrt{s} = 13$ TeV and luminosity 100 fb^{-1} the difference cannot be ignored, there is no difference for the higher energy and luminosity case. We employ in all cases the Poisson probability distribution.

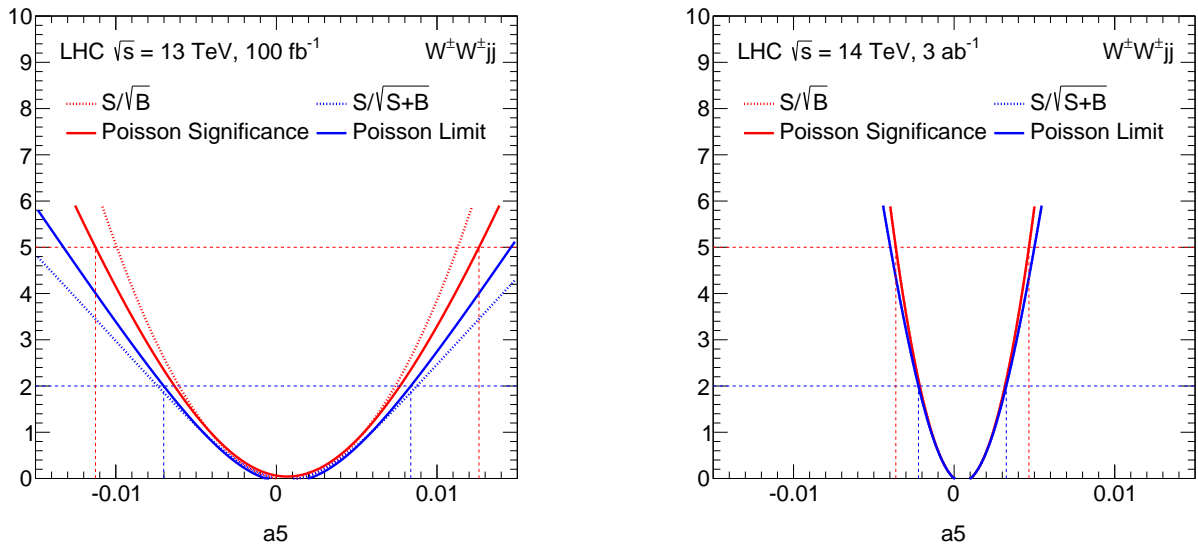


FIG. 6: $\Delta\chi^2$ plot for the coefficient a_5 using the Poisson distribution and the simplified formulas. The plot on the left shows the presence of a discrepancy at low luminosity ($\sqrt{s} = 13$ TeV, luminosity 100 fb^{-1}). The plot on the right shows that there is no discrepancy at higher luminosity ($\sqrt{s} = 14$ TeV, luminosity 3 ab^{-1}) where it is impossible to discriminate the continuous from the dashed lines.

2. Systematic uncertainties

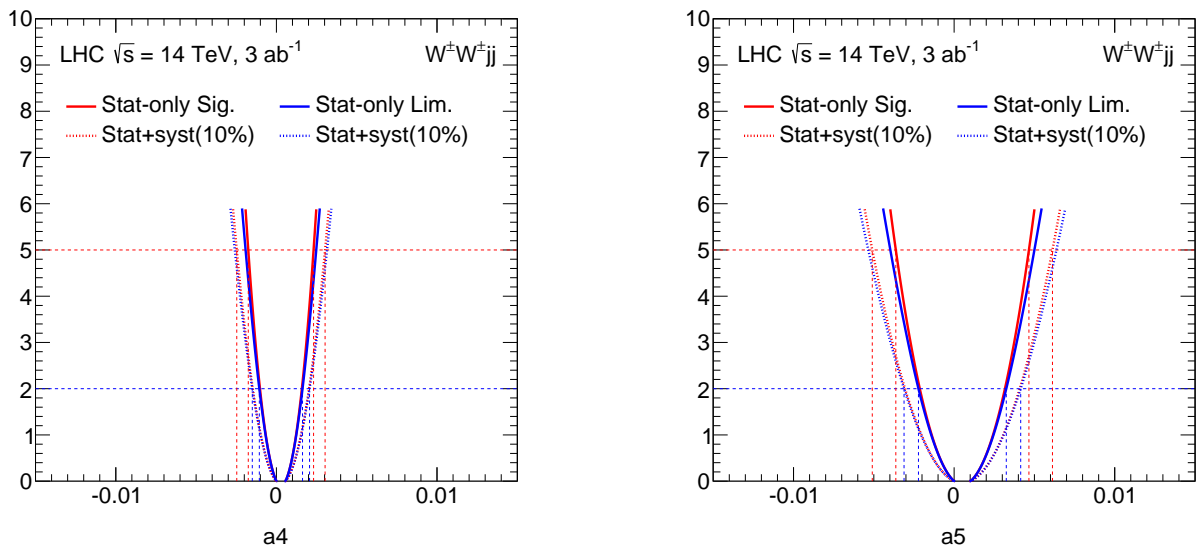


FIG. 7: $\Delta\chi^2$ plot for the coefficient a_4 (left) and a_5 (right) with and without 10% of systematic uncertainty for CM energy $\sqrt{s} = 14$ TeV and luminosity 3 ab^{-1} .

All the results reported in the following are obtained neglecting any systematic uncertainty on the prediction for the number of signal and background events (S and B) because such uncertainties are mostly related to the experimental techniques used to extract the results. To have a feeling of the size of their effect on the results, we have included a non-zero systematic uncertainty on B and compared the limits and the significance with the case without systematics. This comparison is done considering the simplified statistics treatment described above—that is, by considering the formulas S/\sqrt{B} and $S/\sqrt{S+B}$. These two expressions are generalised to the case with non-

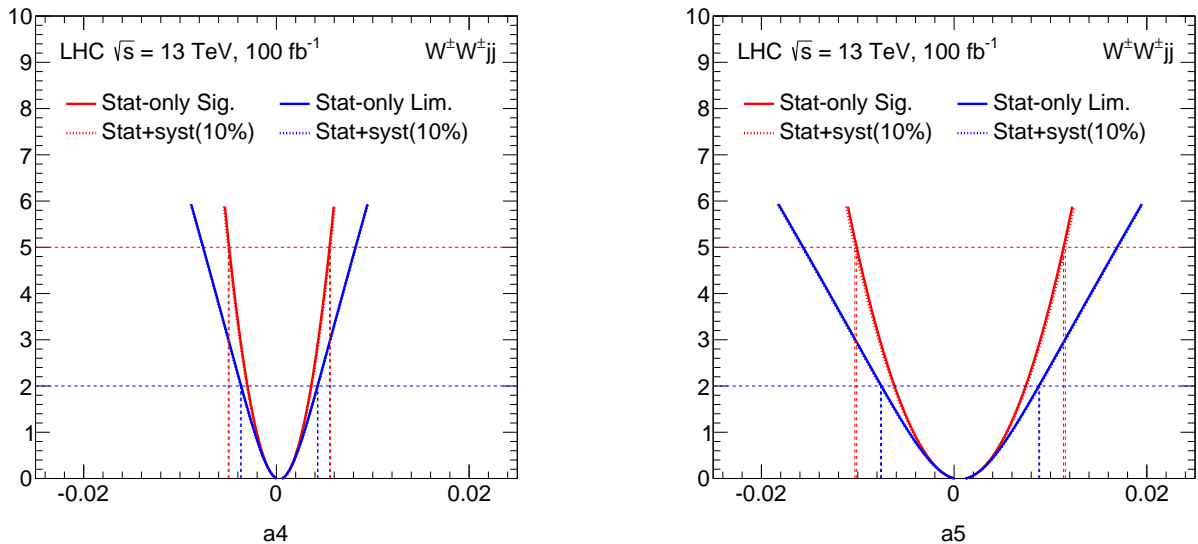


FIG. 8: $\Delta\chi^2$ plot for the coefficient a_4 (left) and a_5 (right) with and without 10% of systematic uncertainty for CM energy $\sqrt{s} = 13$ TeV and luminosity 100 fb^{-1} .

TABLE IV: Upper limits (at 95% CL) for the effective lagrangian coefficients a_4 and a_5 , for two representative CM energies and luminosities, from the channel $W^\pm W^\pm jj$. Comparison with and without the inclusion of a systematic error of 10%.

	$\sqrt{s} = 13 \text{ TeV}, 100 \text{ fb}^{-1}$		$\sqrt{s} = 14 \text{ TeV}, 3 \text{ ab}^{-1}$	
	w/out	w/	w/out	w/
a_4	0.0043	0.0043	0.0016	0.0021
a_5	0.0088	0.0089	0.0032	0.0041

zero systematic uncertainty as $S/\sqrt{B + \delta^2 \cdot B^2}$ and $S/\sqrt{S + B + \delta^2 \cdot B^2}$ respectively, where δ indicate the relative systematic uncertainty on the expected number of background events B .

Table IV (and the corresponding plots in Figs. 7 and 8) show the result of this comparison, performed considering two benchmark CM energy and luminosity scenarios for the two coefficients a_4 and a_5 and a relative systematic uncertainty on B of 10%. The smaller statistical error in the case of CM energy $\sqrt{s} = 14$ TeV and luminosity 3 ab^{-1} makes the systematic error—assumed to remain the same—more important.

As expected, the effect is rather important, especially for large values of integrated luminosity where the Gaussian error is smaller, and one should bear that in mind. Of course, an eventual reduction of such a systematic uncertainty, for instance down at 5%, would proportionally reduce the effect, and, depending on the size of this uncertainty in a real experiment, selection cuts could be further tightened to minimise its impact.

D. Unitarization

For values of the coefficients a , a_2 , a_3 , a_4 and a_5 which are different from the SM ones, the computation of the cross section $\sigma(pp \rightarrow WWjj)$ obtained using the lagrangian in eq. (1) and eq. (5) cannot be trusted because of possible unitarity violation that can arise at the level of some hard scattering diagrams, in particular the ones that involve longitudinal W bosons. In this case, the cross section of the process $W_L W_L \rightarrow W_L W_L$ breaks unitarity at energies larger than the TeV (the exact violation energy depends on the specific values of the coefficients).

This breakdown in unitarity can be understood by looking at the longitudinal W bosons scattering amplitudes in the same- and opposite-sign channel—computed using the equivalence theorem in the isospin limit—can be written

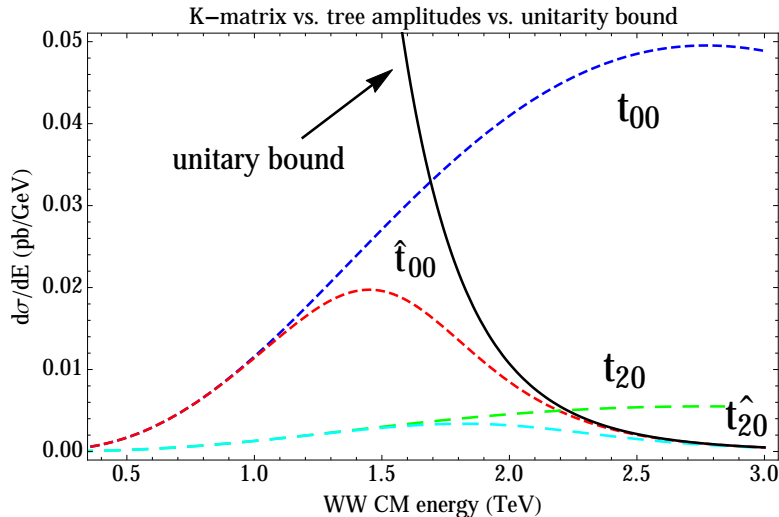


FIG. 9: Cross sections for the scattering of longitudinal W bosons as a function of the CM energy. In green (blue) the contribution of the partial wave t_{20} (t_{00}) for $a_4 = a_5 = 0.001$; in cyan (red) the same result after unitarization by K -matrix. The continuous black line marks the loss of unitarity.

in terms of isospin amplitudes $A_I(s, t)$ as

$$A(W_L^\pm W_L^\pm \rightarrow W_L^\pm W_L^\pm) = A_2 \quad \text{and} \quad A(W_L^\pm W_L^\mp \rightarrow W_L^\pm W_L^\mp) = \frac{1}{3}A_0 + \frac{1}{2}A_1 + \frac{1}{6}A_2. \quad (38)$$

The amplitudes $A_I(s, t)$ can be expanded in terms of partial waves $t_{IJ}(s)$ as

$$A_I(s, t) = 32\pi \sum_{J=0}^{\infty} (2J+1) P_J(\cos\theta) t_{IJ}(s), \quad (39)$$

where

$$t_{IJ}(s) = \frac{1}{64\pi} \int_{-1}^1 d\cos\theta A_I(s, t) P_J(\cos\theta). \quad (40)$$

In our case, at tree level, neglecting partial waves higher than the leading $J = 0$ wave, we have

$$t_{00} = \frac{s}{16\pi v^2} (1 - a^2 + 3g'^2 a_2 + 12g^2 a_3) + \frac{s^2}{12\pi v^4} [11a_5 + 7a_4 - 2g'^2 a_2^2 + 16g^2 a_3^2] \quad (41)$$

$$t_{20} = -\frac{s}{32\pi v^2} (1 - a^2 - 6g'^2 a_2 + 12g^2 a_3) + \frac{s^2}{6\pi v^4} [a_5 + 2a_4 - g'^2 a_2^2 - 4g^2 a_3^2]. \quad (42)$$

The isospin amplitudes $A_I(s, t)$ can then be re-obtained from the partial waves computed above by means of eq. (39). In the approximation of neglecting partial waves higher than $J = 0$, we have very simple relations:

$$A_0(s, t) = 32\pi t_{00}, \quad A_1(s, t) = 0 \quad \text{and} \quad A_2(s, t) = 32\pi t_{20}. \quad (43)$$

An example of such unitarity violation is shown in Fig. 9 where—for values of $a_4 = a_5 = 0.001$ —it occurs around 1.5 and 2 TeV for, respectively, the isospin $I = 0$ and $I = 2$ component.

The amplitudes in eq. (43) violate unitarity and we interpret them as an incomplete approximation to the true amplitudes. One can deal with this problem either by cutting off the collection of events at a given value of the CM energy or by implementing an unitarization procedure.

As an example of the latter, let us look for unitary matrix elements that provides a non-perturbative completion. By inspection of the amplitudes we see that the SS WW channel can only contain double-charged $I = 2$ resonances in the s -channel, the first two being of spin 0 and 2. We assume that these states are sufficiently heavy to be outside the energy reach of LHC. By extension, we assume that no resonance is present within the LHC energy range also in

the opposite-sign WW channel. Therefore, the most appropriated unitarization procedure for our case in which we do not expect resonances is the K -matrix prescription [38]. The K -matrix ansatz consists in using the optical theorem

$$\text{Im } t_{IJ}(s) = |t_{IJ}(s)|^2 \quad (44)$$

in order to impose the following condition on the unitarized partial wave $\hat{t}_{IJ}(s)$

$$\text{Im } \frac{1}{\hat{t}_{IJ}(s)} = -1. \quad (45)$$

The K -matrix unitarized partial wave is then defined to be

$$\hat{t}_{IJ}(s) = \frac{t_{IJ}(s)}{1 - it_{IJ}(s)}, \quad (46)$$

where $t_{IJ}(s)$ is the tree-level partial wave amplitude. The quantity $\hat{t}_{IJ}(s, t)$ satisfies by construction the optical theorem and is supposed to represent a re-summation of the higher order terms whose contribution restore unitarity. The result of this unitarization is shown in Fig. 9 and compared to the tree-level result.

If we define the rescaling factor for the SS WW events

$$r_{++}(s, a_3, a_4, a_5) = \frac{|\hat{t}_{20}|^2}{|t_{20}|^2}, \quad (47)$$

we can use it to re-weight the events that survive after having applied all the selection cuts, in order to obtain a result that satisfies the unitarity bound. This procedure is reliable if the events that survive after the selection cuts are dominated by the production of longitudinal polarized W .

TABLE V: Comparison of upper exclusion limits (at 95% and 99% CL) and discovery significance (at 3 and 5 σ) for the effective lagrangian coefficients a_4 and a_5 , for CM energy $\sqrt{s} = 14$ TeV and luminosity 300 fb^{-1} , using the K -matrix and the sharp cut off unitarization procedures. Values obtained by using the SS WW channel.

$\sqrt{s} = 14 \text{ TeV}, 300 \text{ fb}^{-1}$				
K -matrix			sharp cut off ($E_{WW} < 2 \text{ TeV}$)	
	95% (99%)	3 σ (5 σ)	95% (99%)	3 σ (5 σ)
a_4	0.0028 (0.0038)	0.0035 (0.0053)	0.0027 (0.0034)	0.0032 (0.0041)
a_5	0.0053 (0.0072)	0.0066 (0.0107)	0.0055 (0.0068)	0.0064 (0.0084)

The K -matrix ansatz and the cut off in energy are two possible procedures to deal with the violation of unitarity. Table V shows that the two procedures (for an appropriate choice of cut off) are substantially equivalent. Their differences quantify the dependence on the unitarization procedure of the limits.

Because it is more difficult to define a rescaling for the OS channel as done above for the SS channel, and because of the additional assumptions entering the K -matrix procedure, we follow the simplest procedure and introduce a sharp cut off in the data collection so as to make the amplitudes unitarity.

The cut off must be chosen to be less than $4\pi v$, the limit for the chiral lagrangian expansion, and below the range in which the growth becomes too fast. We take $m_{WW} < 1.25 \text{ TeV}$ for the SS channel and $< 2 \text{ TeV}$ for the OS channel. It can be shown that for these values, as in Table V, differences between the two unitarization procedures are minimal.

III. RESULTS

As discussed in section II A, we have generated events in which the coefficients of the effective lagrangians in eq. (1) and eq. (5) of section IB, parameterising deviations from the SM, were allowed to vary. We consider only the coefficients a , a_2 , a_3 , a_4 and a_5 because the coefficient a_1 is already severely constrained by LEP data, as discussed in section IE, and we assume it vanishing in our analysis. The coefficients a_4 and a_5 , according to our discussion in section IC, are the leading and most important ones. They should be searched first. Once they have been constrained, the simulation for the coefficients a_2 , a_3 and a can be carried out after setting a_4 and a_5 equal to zero.

We report in Tables VI-IX the results in terms of exclusion limits (95 and 99% CL) and discovery significance (3 and 5σ)—as discussed in section II C—for the benchmark luminosities of 100 and 300 fb^{-1} (at CM energy of $\sqrt{s} = 13\text{ TeV}$) and 300 fb^{-1} and 3 ab^{-1} (at $\sqrt{s} = 14\text{ TeV}$). All coefficients are here varied one at the time.

As it can be seen from Tables VI-IX, the OS channel does not provide stronger limits for any of the coefficients and the SS channel is sufficient by itself in setting the most stringent constraints.

Figs. 10 and 11 show the exclusion limits (95% CL) and discovery significance (5σ) for the coefficients a_4 and a_5 obtained from the SS and OS WW channels for, respectively CM energy $\sqrt{s} = 13$ and 14 TeV and the benchmark luminosities. The coefficients a_4 and a_5 are now varied simultaneously.

TABLE VI: Exclusion limits (at 95% and 99% CL) and discovery significance (at 3 and 5σ) for the effective lagrangian coefficients a_5 , a_4 , a_3 , a_2 and a for CM energy $\sqrt{s} = 13\text{ TeV}$ and two benchmark luminosities for LHC run 2. Values obtained by varying the coefficients one at the time. All limits are obtained from the $W^\pm W^\pm jj$ SS channel.

$\sqrt{s} = 13\text{ TeV}$ ($W^\pm W^\pm jj$ SS channel)					
		100 fb^{-1}		300 fb^{-1}	
		95% (99%)	3σ (5σ)	95% (99%)	3σ (5σ)
a_5		+0.0084 (+0.0105)	+0.0095 (+0.0126)	+0.0062 (+0.0077)	+0.0072 (+0.0094)
		-0.007 (-0.0092)	-0.0082 (-0.0113)	-0.0049 (-0.0063)	-0.0059 (-0.008)
a_4		+0.0041 (+0.0052)	+0.0047 (+0.0062)	+0.003 (+0.0037)	+0.0035 (+0.0046)
		-0.0035 (-0.0046)	-0.004 (-0.0056)	-0.0024 (-0.0031)	-0.0029 (-0.004)
a_3		+0.097 (+0.121)	+0.109 (+0.143)	+0.074 (+0.089)	+0.085 (+0.108)
		-0.072 (-0.096)	-0.085 (-0.118)	-0.049 (-0.065)	-0.060 (-0.083)
a_2		+1.63 (+2.03)	+1.84 (+2.41)	+1.24 (+1.5)	+1.42 (+1.82)
		-1.21 (-1.61)	-1.42 (-1.99)	-0.82 (-1.09)	-1.01 (-1.4)
a		+1.52 (+1.6)	+1.56 (+1.68)	+1.43 (+1.49)	+1.47 (+1.56)
		0.17 (-0.44)	-0.11 (-1.57)	0.54 (0.31)	0.39 (-0.07)

TABLE VII: Exclusion limits (at 95% and 99% CL) and discovery significance (at 3 and 5σ) for the effective lagrangian coefficients a_5 , a_4 , a_3 , a_2 and a for CM energy $\sqrt{s} = 14\text{ TeV}$ and two benchmark luminosities for LHC run 3. Values obtained by varying the coefficients one at the time. All limits are obtained from the $W^\pm W^\pm jj$ SS channel.

$\sqrt{s} = 14\text{ TeV}$ ($W^\pm W^\pm jj$ SS channel)					
		300 fb^{-1}		3 ab^{-1}	
		95% (99%)	3σ (5σ)	95% (99%)	3σ (5σ)
a_5		+0.0055 (+0.0068)	+0.0064 (+0.0084)	+0.0032 (+0.0039)	+0.0037 (+0.0047)
		-0.0045 (-0.0058)	-0.0054 (-0.0074)	-0.0022 (-0.0029)	-0.0027 (-0.0036)
a_4		+0.0027 (+0.0034)	+0.0032 (+0.0041)	+0.0016 (+0.0019)	+0.0019 (+0.0023)
		-0.0022 (-0.0028)	-0.0026 (-0.0036)	-0.0011 (-0.0014)	-0.0013 (-0.0018)
a_3		+0.073 (+0.089)	+0.084 (+0.108)	+0.046 (+0.054)	+0.052 (+0.063)
		-0.050 (-0.065)	-0.061 (-0.084)	-0.023 (-0.030)	-0.028 (-0.039)
a_2		+1.14 (+1.37)	+1.30 (+1.64)	+0.75 (+0.86)	+0.83 (+0.99)
		-0.70 (-0.93)	-0.86 (-1.21)	-0.31 (-0.42)	-0.39 (-0.55)
a		+1.37 (+1.43)	+1.42 (+1.5)	+1.27 (+1.3)	+1.29 (+1.33)
		0.64 (0.47)	0.52 (0.22)	0.86 (0.81)	0.82 (0.73)

TABLE VIII: *Exclusion limits (at 95% and 99% CL) and discovery significance (at 3 and 5 σ) for the effective lagrangian coefficients a_5 , a_4 , a_3 , a_2 and a for CM energy $\sqrt{s} = 13$ TeV and two benchmark luminosities for LHC run 2. Values obtained by varying the coefficients one at the time. All limits are obtained from the $W^\pm W^\mp jj$ OS channel.*

$\sqrt{s} = 13$ TeV ($W^\pm W^\mp jj$ OS channel)				
100 fb $^{-1}$			300 fb $^{-1}$	
	95% (99%)	3 σ (5 σ)	95% (99%)	3 σ (5 σ)
a_5	+0.0089 (+0.0114)	+0.0105 (+0.0141)	+0.0064 (+0.0081)	+0.0077 (+0.0103)
	-0.0095 (-0.012)	-0.011 (-0.0147)	-0.007 (-0.0087)	-0.0083 (-0.0109)
a_4	+0.0141 (+0.0179)	+0.0165 (+0.0221)	+0.0103 (+0.0129)	+0.0123 (+0.0162)
	-0.014 (-0.0178)	-0.0164 (-0.022)	-0.0102 (-0.0128)	-0.0122 (-0.0161)
a_3	+0.198 (+0.245)	+0.227 (+0.295)	+0.152 (+0.183)	+0.176 (+0.224)
	-0.149 (-0.195)	-0.178 (-0.246)	-0.103 (-0.134)	-0.127 (-0.174)
a_2	+1.17 (+1.48)	+1.36 (+1.81)	+0.87 (+1.07)	+1.03 (+1.34)
	-1.07 (-1.37)	-1.26 (-1.70)	-0.77 (-0.97)	-0.92 (-1.24)
a	+1.83 (+2.08)	+1.99 (+2.35)	+1.58 (+1.75)	+1.71 (+1.97)
	-0.41 (-0.65)	-0.56 (-0.92)	-0.19 (-0.34)	-0.30 (-0.54)

TABLE IX: *Exclusion limits (at 95% and 99% CL) and discovery significance (at 3 and 5 σ) for the effective lagrangian coefficients a_5 , a_4 , a_3 , a_2 and a for CM energy $\sqrt{s} = 14$ TeV and two benchmark luminosities for LHC run 3. Values obtained by varying the coefficients one at the time. All limits are obtained from the $W^\pm W^\mp jj$ OS channel.*

$\sqrt{s} = 14$ TeV ($W^\pm W^\mp jj$ OS channel)				
300 fb $^{-1}$			3 ab $^{-1}$	
	95% (99%)	3 σ (5 σ)	95% (99%)	3 σ (5 σ)
a_5	+0.0061 (+0.0077)	+0.0073 (+0.0097)	+0.0033 (+0.0041)	+0.004 (+0.0052)
	-0.0062 (-0.0077)	-0.0074 (-0.0098)	-0.0034 (-0.0042)	-0.0041 (-0.0052)
a_4	+0.0084 (+0.0107)	+0.0102 (+0.0136)	+0.0043 (+0.0055)	+0.0053 (+0.007)
	-0.0097 (-0.012)	-0.0115 (-0.0149)	-0.0056 (-0.0068)	-0.0066 (-0.0083)
a_3	+0.134 (+0.165)	+0.158 (+0.205)	+0.077 (+0.094)	+0.091 (+0.114)
	-0.115 (-0.146)	-0.140 (-0.187)	-0.059 (-0.075)	-0.072 (-0.096)
a_2	+0.75 (+0.93)	+0.89 (+1.17)	+0.42 (+0.52)	+0.50 (+0.64)
	-0.71 (-0.89)	-0.85 (-1.13)	-0.38 (-0.47)	-0.45 (-0.59)
a	+1.56 (+1.67)	+1.64 (+1.81)	+1.36 (+1.41)	+1.40 (+1.49)
	-0.50 (-1.35)	-1.15 (-2.74)	0.55 (0.31)	0.36 (-0.06)

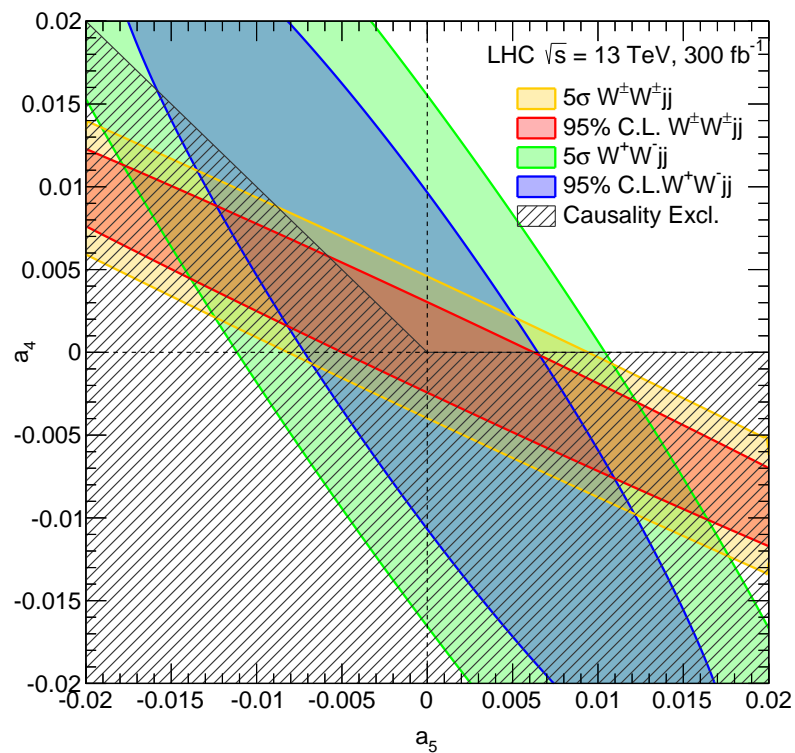
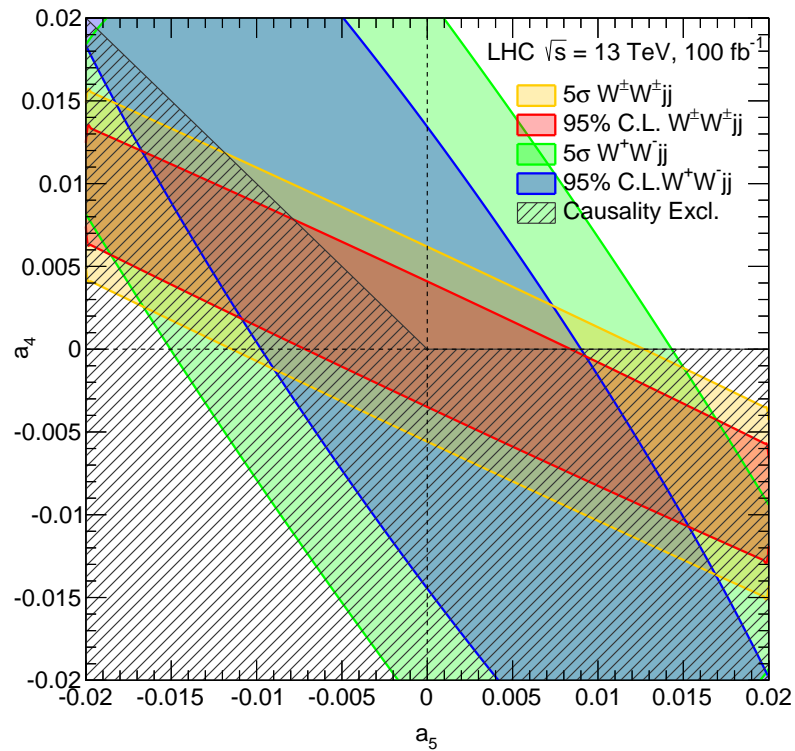


FIG. 10: Exclusion limits (at 95% CL) and discovery significance (5σ) for the effective lagrangian coefficients a_4 and a_5 at CM energy $\sqrt{s} = 13$ TeV from the same-sign (in yellow/orange) and opposite-sign (in light green/blue) channels. Hatched in grey the area where causality would be violated.

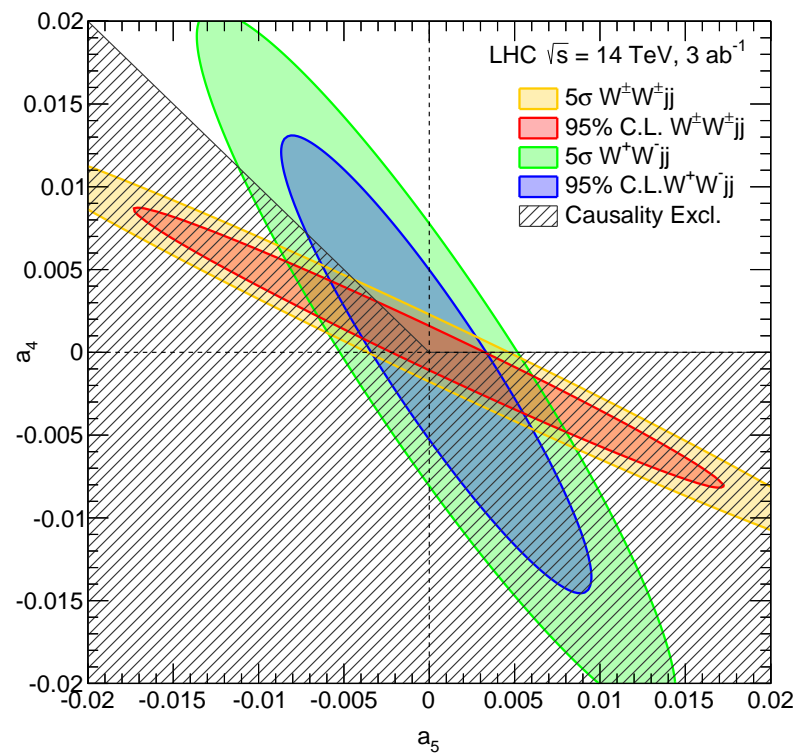
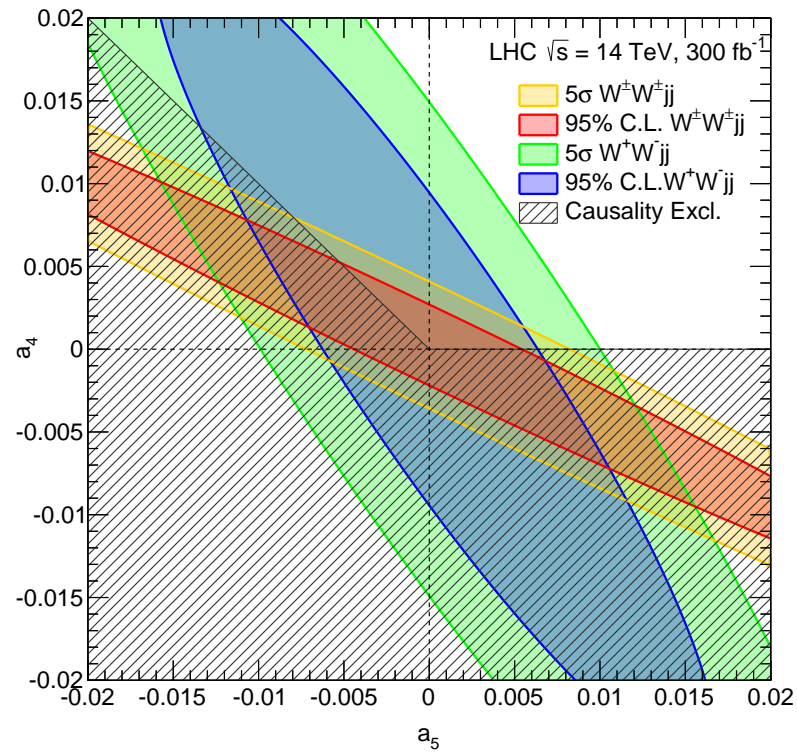


FIG. 11: Same as in Fig. 10 for CM energy $\sqrt{s} = 14$ TeV.

IV. DISCUSSION

While the presence of resonances is the most dramatic signal for a strongly interacting sector, they may be too heavy or broad to be clearly seen at the LHC. The discovery of a non-vanishing coefficient of the effective lagrangian in eq. (5), introduced in section IB, is a more systematic way to search for the presence of the strongly interacting sector behind the breaking of the EW symmetry. In addition, exclusion limits provide an indirect indication about the energy scale of the masses of those resonances that are expected from such new interactions.

The identification of the most appropriated selection cuts is crucial but it is now well understood that—in addition to the central jet veto necessary to remove the QCD background—the control of the large EW background can be achieved by means of a selection on the transverse momenta of the jets and final leptons.

We have shown that a significant improvement in both discovery significance and exclusion limits for the chiral effective lagrangian coefficients a_4 and a_5 can be expected from the current and the next run of the LHC. Already at CM energy $\sqrt{s} = 13$ TeV and a luminosity of 100 fb^{-1} the limits will reach the permil precision thus coming within range of the values expected by purely dimensional analysis. These results can be obtained by studying the $SS WW \rightarrow WW$ channel alone.

The determination of the coefficient a_3 within VBS—the best limits for which come at the moment from precision measurements—will become competitive already at the LHC run 2 when a luminosity of 300 fb^{-1} will be available. The coefficient a_2 gives rise to smaller deviations in VBS and is determined with less precision; its constraints will be competitive with those from TGC data at LEP only when higher luminosities become available.

Finally, the coefficient a —controlling the coupling of the Higgs to the vector bosons in eq. (1) in section IB—remains best determined in the decay processes of the Higgs boson. Only at future LHC runs a comparable limit will be available from VBS.

While VBS remains our best laboratory to study EW symmetry breaking, the presence of systematic errors hard to reduce and even estimate will eventually limit the final precision of the measurements that can be achieved at the LHC. The same is true for the study of the Higgs boson decays and the complementary determination of the coefficient a , as defined in eq. (1) in section IB.

Acknowledgments

We thank Francesco Riva for discussions. MF is associated to SISSA. The work of AT is supported by the São Paulo Research Foundation (FAPESP) under grants 2011/11973-4 and 2013/02404-1. The work of MP and AU is supported by the ERC Advanced Grant n. 267985, “Electroweak Symmetry Breaking, Flavour and Dark Matter: One Solution for Three Mysteries” (DaMeSyFla).

-
- [1] G. Aad *et al.* [ATLAS Collaboration], Phys. Lett. B **716**, 1 (2012) [[arXiv:1207.7214](#) [hep-ex]]; S. Chatrchyan *et al.* [CMS Collaboration], Phys. Lett. B **716**, 30 (2012) [[arXiv:1207.7235](#) [hep-ex]].
 - [2] M. S. Chanowitz and M. K. Gaillard, Nucl. Phys. B **261**, 379 (1985).
 - [3] T. Appelquist and C. W. Bernard, Phys. Rev. D **22**, 200 (1980); A. C. Longhitano, Phys. Rev. D **22**, 1166 (1980); T. Appelquist and G. H. Wu, Phys. Rev. D **48**, 3235 (1993) [[hep-ph/9304240](#)].
 - [4] D. Espriu and B. Yencho, Phys. Rev. D **87**, no. 5, 055017 (2013) [[arXiv:1212.4158](#) [hep-ph]]; D. Espriu and F. Mescia, Phys. Rev. D **90**, no. 1, 015035 (2014) [[arXiv:1403.7386](#) [hep-ph]].
 - [5] R. L. Delgado, A. Dobado and F. J. Llanes-Estrada, J. Phys. G **41**, 025002 (2014) [[arXiv:1308.1629](#) [hep-ph]]; R. L. Delgado, A. Dobado and F. J. Llanes-Estrada, [arXiv:1412.3277](#) [hep-ph]; R. L. Delgado, A. Dobado and F. J. Llanes-Estrada, Phys. Rev. D **91**, no. 7, 075017 (2015) [[arXiv:1502.04841](#) [hep-ph]].
 - [6] K. Doroba, J. Kalinowski, J. Kuczmarzski, S. Pokorski, J. Rosiek, M. Szeleper and S. Tkaczyk, Phys. Rev. D **86**, 036011 (2012) [[arXiv:1201.2768](#) [hep-ph]].
 - [7] D. A. Dicus and R. Vega, Phys. Rev. Lett. **57**, 1110 (1986); M. J. Duncan, G. L. Kane and W. W. Repko, Nucl. Phys. B **272**, 517 (1986).
 - [8] V. D. Barger, K. m. Cheung, T. Han and R. J. N. Phillips, Phys. Rev. D **42**, 3052 (1990); J. Bagger, V. D. Barger, K. m. Cheung, J. F. Gunion, T. Han, G. A. Ladinsky, R. Rosenfeld and C.-P. Yuan, Phys. Rev. D **52**, 3878 (1995) [[hep-ph/9504426](#)].
 - [9] J. Bagger, V. D. Barger, K. m. Cheung, J. F. Gunion, T. Han, G. A. Ladinsky, R. Rosenfeld and C.-P. Yuan, Phys. Rev. D **52**, 3878 (1995) [[hep-ph/9504426](#)].
 - [10] J. M. Butterworth, B. E. Cox and J. R. Forshaw, Phys. Rev. D **65**, 096014 (2002) [[hep-ph/0201098](#)].
 - [11] A. Alboteanu, W. Kilian and J. Reuter, JHEP **0811**, 010 (2008) [[arXiv:0806.4145](#) [hep-ph]]; T. Han, D. Krohn, L. T. Wang and W. Zhu, JHEP **1003**, 082 (2010) [[arXiv:0911.3656](#) [hep-ph]]. C. Englert, B. Jager, M. Worek and D. Zeppenfeld, Phys.

- Rev. D **80**, 035027 (2009); A. Freitas and J. S. Gainer, Phys. Rev. D **88**, no. 1, 017302 (2013) [[arXiv:1212.3598](#)]; W. Kilian, T. Ohl, J. Reuter and M. Sekulla, Phys. Rev. D **91**, 096007 (2015) [[arXiv:1408.6207](#) [hep-ph]].
- [12] E. Accomando, A. Ballestrero, S. Bolognesi, E. Maina and C. Mariotti, JHEP **0603**, 093 (2006) [[hep-ph/0512219](#)]; A. Ballestrero, G. Bevilacqua and E. Maina, JHEP **0905**, 015 (2009) [[arXiv:0812.5084](#) [hep-ph]]; A. Ballestrero, G. Bevilacqua, D. B. Franzosi and E. Maina, JHEP **0911**, 126 (2009) [[arXiv:0909.3838](#) [hep-ph]].
- [13] S. Godfrey, AIP Conf. Proc. **350**, 209 (1995) [[hep-ph/9505252](#)]; A. S. Belyaev, O. J. P. Eboli, M. C. Gonzalez-Garcia, J. K. Mizukoshi, S. F. Novaes and I. Zacharov, Phys. Rev. D **59**, 015022 (1999) [[hep-ph/9805229](#)].
- [14] A. Dobado, M. J. Herrero and J. Terron, Z. Phys. C **50**, 205 (1991); A. Dobado, M. J. Herrero, J. R. Pelaez, E. Ruiz Morales and M. T. Urdiales, Phys. Lett. B **352**, 400 (1995) [[hep-ph/9502309](#)].
- [15] M. Fabbrichesi and L. Vecchi, Phys. Rev. D **76**, 056002 (2007) [[hep-ph/0703236](#)].
- [16] I. Brivio, T. Corbett, O. J. P. Eboli, M. B. Gavela, J. Gonzalez-Fraile, M. C. Gonzalez-Garcia, L. Merlo and S. Rigolin, JHEP **1403**, 024 (2014) [[arXiv:1311.1823](#) [hep-ph]].
- [17] O. J. P. Eboli, M. C. Gonzalez-Garcia and J. K. Mizukoshi, Phys. Rev. D **74**, 073005 (2006) [[hep-ph/0606118](#)].
- [18] M. Szleper, [arXiv:1412.8367](#) [hep-ph].
- [19] A. Manohar and H. Georgi, Nucl. Phys. B **234**, 189 (1984); H. Georgi and L. Randall, Nucl. Phys. B **276**, 241 (1986); G. F. Giudice, C. Grojean, A. Pomarol and R. Rattazzi, JHEP **0706**, 045 (2007) [[hep-ph/0703164](#)].
- [20] M. E. Peskin and T. Takeuchi, Phys. Rev. Lett. **65**, 964 (1990); M. Golden and L. Randall, Nucl. Phys. B **361**, 3 (1991); B. Holdom and J. Terning, Phys. Lett. B **247**, 88 (1990).; M. E. Peskin and T. Takeuchi, Phys. Rev. D **46**, 381 (1992); G. Altarelli and R. Barbieri, Phys. Lett. B **253**, 161 (1991); G. Altarelli, R. Barbieri and S. Jadach, Nucl. Phys. B **369**, 3 (1992) [Erratum-ibid. B **376**, 444 (1992)].
- [21] R. Barbieri, A. Pomarol and R. Rattazzi, Phys. Lett. B **591**, 141 (2004) [[hep-ph/0310285](#)]; R. Barbieri, A. Pomarol, R. Rattazzi and A. Strumia, Nucl. Phys. B **703**, 127 (2004) [[hep-ph/0405040](#)].
- [22] K. Hagiwara, S. Ishihara, R. Szalapski and D. Zeppenfeld, Phys. Lett. B **283**, 353 (1992).
- [23] See, e.g.: A. Falkowski and F. Riva, JHEP **1502**, 039 (2015) [[arXiv:1411.0669](#) [hep-ph]].
- [24] J. Elias-Mir, J. R. Espinosa, E. Masso and A. Pomarol, JHEP **1308**, 033 (2013) [[arXiv:1302.5661](#) [hep-ph]].
- [25] W. Buchmuller and D. Wyler, Nucl. Phys. B **268**, 621 (1986); B. Grzadkowski, M. Iskrzynski, M. Misiak and J. Rosiek, JHEP **1010**, 085 (2010) [[arXiv:1008.4884](#) [hep-ph]].
- [26] M. Baak, A. Blondel, A. Bodek, R. Caputo, T. Corbett, C. Degrande, O. Eboli and J. Erler *et al.*, [arXiv:1310.6708](#) [hep-ph].
- [27] A. Falkowski, F. Riva and A. Urbano, JHEP **1311**, 111 (2013) [[arXiv:1303.1812](#) [hep-ph]].
- [28] S. Schael *et al.* [ALEPH Collaboration], Phys. Lett. B **614**, 7 (2005); P. Achard *et al.* [L3 Collaboration], Phys. Lett. B **586**, 151 (2004) [[hep-ex/0402036](#)]; G. Abbiendi *et al.* [OPAL Collaboration], Eur. Phys. J. C **33**, 463 (2004) [[hep-ex/0308067](#)].
- [29] T. N. Pham and T. N. Truong, Phys. Rev. D **31**, 3027 (1985); A. Adams, N. Arkani-Hamed, S. Dubovsky, A. Nicolis and R. Rattazzi, JHEP **0610**, 014 (2006) [[hep-th/0602178](#)]; J. Distler, B. Grinstein, R. A. Porto and I. Z. Rothstein, Phys. Rev. Lett. **98**, 041601 (2007) [[hep-ph/0604255](#)]; L. Vecchi, JHEP **0711**, 054 (2007) [[arXiv:0704.1900](#) [hep-ph]].
- [30] G. Aad *et al.* [ATLAS Collaboration], Phys. Rev. Lett. **113**, no. 14, 141803 (2014) [[arXiv:1405.6241](#) [hep-ex]]; CMS Collaboration [CMS Collaboration], CMS-PAS-SMP-13-015.
- [31] C. Degrande, J. L. Holzbauer, S.-C. Hsu, A. V. Kotwal, S. Li, M. Marx, O. Mattelaer and J. Metcalfe *et al.*, [arXiv:1309.7452](#) [physics.comp-ph].
- [32] J. Ellis and T. You, JHEP **1306**, 103 (2013) [[arXiv:1303.3879](#) [hep-ph]].
- [33] See, for example: [CMS Collaboration], [arXiv:1307.7135](#).
- [34] N. D. Christensen and C. Duhr, Comput. Phys. Commun. **180** (2009) 1614 [[arXiv:0806.4194](#) [hep-ph]].
- [35] J. Alwall *et al.*, JHEP **1106**, 128 (2011) [[arXiv:1106.052211](#) [hep-ph]].
- [36] T. Sjostrand, S. Mrenna and P. Z. Skands, JHEP **0605**, 026 (2006) [[hep-ph/0603175](#)].
- [37] J. de Favereau *et al.* [DELPHES 3 Collaboration], JHEP **1402**, 057 (2014) [[arXiv:1307.6346](#) [hep-ex]].
- [38] J. S. Schwinger, Phys. Rev. **74**, 1439 (1948); S. N. Gupta, Proc. Phys. Soc. A **63**, 681 (1950).